



Discovery and optimization of 2-((1*H*-indol-3-yl)thio)-*N*-benzyl-acetamides as novel SARS-CoV-2 RdRp inhibitors

Guo-Ning Zhang¹, Jianyuan Zhao¹, Quanjie Li¹, Minghua Wang, Mei Zhu, Juxian Wang^{**}, Shan Cen^{***}, Yucheng Wang^{*}

Institute of Medicinal Biotechnology, Chinese Academy of Medical Science and Peking Union Medical College, Beijing, 100050, China

ARTICLE INFO

Article history:

Received 13 January 2021

Received in revised form

20 May 2021

Accepted 4 June 2021

Available online 10 June 2021

Keywords:

SARS-CoV-2

COVID-19

RdRp inhibitor

2-((Indol-3-yl)thio)-*N*-Benzyl-acetamides

ABSTRACT

The emerging severe acute respiratory syndrome coronavirus 2 (SARS-CoV-2) is responsible for the global pandemic coronavirus disease (COVID-19), but no specific antiviral drug has been proven effective for controlling this pandemic to date. In this study, several 2-((indol-3-yl)thio)-*N*-benzyl-acetamides were identified as SARS-CoV-2 RNA-dependent RNA polymerase (RdRp) inhibitors. After a two-round optimization, a new series of 2-((indol-3-yl)thio)-*N*-benzyl-acetamides was designed, synthesized, and evaluated for SARS-CoV-2 RdRp inhibitory effect. Compounds **6b2**, **6b5**, **6c9**, **6d2**, and **6d5** were identified as potent inhibitors with IC₅₀ values of 3.35 ± 0.21 μM, 4.55 ± 0.2 μM, 1.65 ± 0.05 μM, 3.76 ± 0.79 μM, and 1.11 ± 0.05 μM, respectively; the IC₅₀ of remdesivir (control) was measured as 1.19 ± 0.36 μM. All of the compounds inhibited RNA synthesis by SARS-CoV-2 RdRp. The most potent compound **6d5**, which showed a stronger inhibitory activity against the human coronavirus HCoV-OC43 than remdesivir, is a promising candidate for further investigation.

© 2021 Elsevier Masson SAS. All rights reserved.

1. Introduction

Humans are currently affected by the coronavirus disease (COVID-19) pandemic, caused by the emergence of severe acute respiratory syndrome coronavirus 2 (SARS-CoV-2), resulting in ~160 million infections and more than 3.3 million deaths worldwide (until May 13, 2021) [1]. To date, no specific antiviral drug has been approved to treat the infection caused by this coronavirus. Furthermore, the interim results of the largest clinical trial of anti-COVID-19 drugs to date show that the four most promising candidate therapies, namely remdesivir [2–4], hydroxychloroquine [5], lopinavir/ritonavir [6], and interferon-β1a [7], have little effect on the 28-day mortality or hospitalization course of hospitalized patients. Although vaccines are officially approved for the prevention of COVID-19 and massive vaccination has begun in many countries, infections are still increasing worldwide [8,9]. It is believed that SARS-CoV-2 may persist among humans for a long

time [10], regardless of the availability of effective vaccines. Therefore, there is an urgent need to identify novel and efficient anti-COVID-19 drugs.

SARS-CoV-2 belongs to the Coronaviridae family and is a positive-sense single-stranded RNA betacoronavirus [11–13]. In addition to SARS-CoV-2, six other human coronaviruses—HCoV-229E, HCoV-OC43, HCoV-NL63, HCoV-HKU1, severe acute respiratory syndrome coronavirus (SARS-CoV), and Middle East respiratory syndrome coronavirus (MERS-CoV)—have been identified previously [14,15]. HCoV-229E, HCoV-OC43, HCoV-NL63, and HCoV-HKU1 usually only evoke mild cold-like symptoms [16,17]; hence, they are commonly used as drug screening tools for viral infectious diseases [18].

RNA-dependent RNA polymerase (RdRp), which mediates the transcription and replication of the RNA genome during infection, is a crucial enzyme in the life cycle of most RNA viruses, except retroviruses [19,20]. The fact that this enzyme has no human counterpart, together with its essentiality for the life cycle of the virus, improves its potential as a drug target for antiviral development. Thus, this is a very active field of research and a hot topic for pharmaceutical companies and academic research groups [21–25].

A number of antiviral drugs, such as sofosbuvir, fapiravir, ribavirin, beclabuvir, and dasabuvir (Fig. 1), are in clinical use for different viruses (e.g., hepatitis C [26–28], influenza [29], and

* Corresponding author.

** Corresponding author.

*** Corresponding author.

E-mail addresses: wangjuxian@imb.pumc.edu.cn (J. Wang), shancen@imb.pumc.edu.cn (S. Cen), wangyucheng@imb.pumc.edu.cn (Y. Wang).

¹ These authors contributed equally to this work.

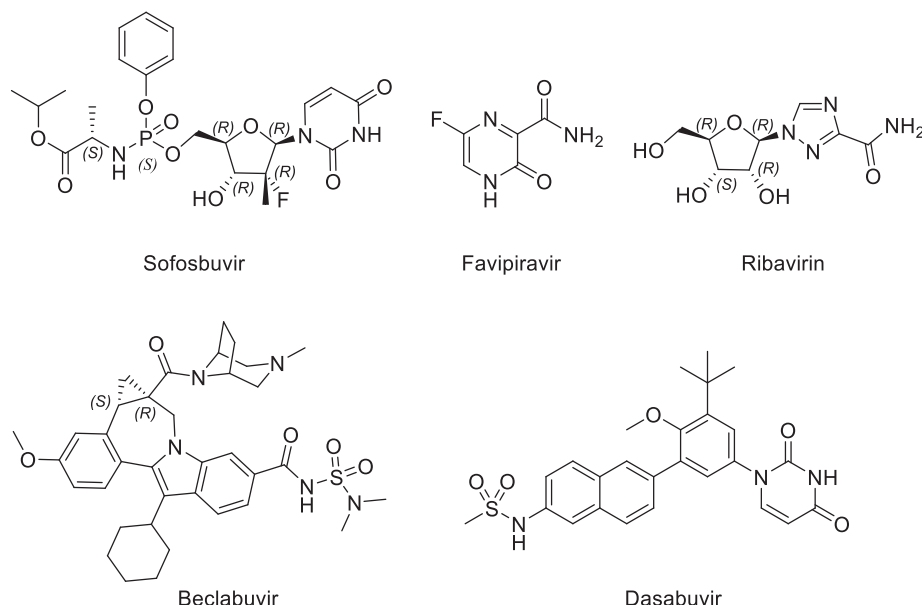


Fig. 1. Structure of FDA-approved antivirals targeting RdRp.

respiratory syncytial [30] viruses) on the basis of their *anti*-RdRp activity [31,32]. Further, dozens of RdRp inhibitors are undergoing clinical trials, which were comprehensively summarized by Tian et al. in January 2021 [33]. In addition to the approved indications, most RdRp inhibitors have also been studied for the treatment of other viral infections [34].

In our previous work, we have reported a series of 2-((1*H*-indol-3-yl)thio)-*N*-phenyl-acetamides (Fig. 2) as novel dual inhibitors of respiratory syncytial virus (RSV) and influenza A virus (IAV) with sub-micromolar EC₅₀ values; the mechanism study further suggested that these compounds act as RdRp inhibitors [35,36]. Considering that the RdRp structure is highly conserved in RNA

viruses, these compounds were evaluated for their SARS-CoV-2 RdRp inhibitory effect in a cell-based Gaussia luciferase (Gluc) reporter assay. Notably, most compounds showed moderate inhibitory activity (15%–40%) at a concentration of 10 μM; however, an increased inhibitory effect was observed when substituted aniline was replaced with benzylamine (**6a1**) or 2-methoxybenzylamine (**6a5**) (Fig. 2). Thus, a new series of 2-((indol-3-yl)thio)-*N*-benzyl-acetamides was synthesized and evaluated for its SARS-CoV-2 RdRp inhibitory effect in the Gluc reporter system. After a two-round optimization, compounds **6b2**, **6b5**, **6c9**, **6d2**, and **6d5** were identified as potent RdRp inhibitors with IC₅₀ values of 3.35 ± 0.21 μM, 4.55 ± 0.2 μM, 1.65 ± 0.05 μM, 3.76 ± 0.79 μM, and

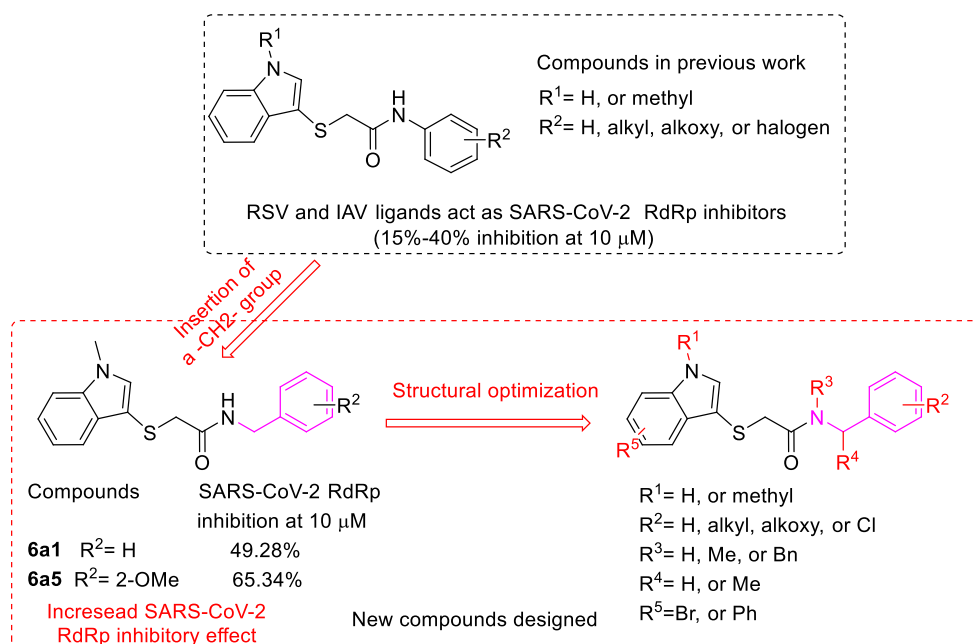


Fig. 2. Previously identified SARS-CoV-2 RdRp inhibitors and newly designed compounds.

$1.11 \pm 0.05 \mu\text{M}$, respectively; the IC_{50} of the positive control remdesivir was measured as $1.19 \pm 0.36 \mu\text{M}$. All the selected compounds **6b2**, **6b5**, **6c9**, **6d2**, and **6d5** showed dose-dependent inhibition of SARS-CoV-2 RdRp, and the activity was comparable to that of remdesivir. They inhibit the efficiency of SARS-CoV-2 RdRp-mediated RNA synthesis and diminish both plus- and minus-strand Gluc RNA level more potently than remdesivir. All the tested compounds showed good tolerance to nps14/nsp10 exoribonuclease, which is necessary for their efficacy in vivo. Finally, compound **6d5** was selected to evaluate its antiviral effect against HCoV-OC43 and HCoV-NL63; it was identified as the most potent candidate with a stronger inhibitory activity than remdesivir in vivo.

2. Results and discussion

The synthetic schemes for compounds **6a-d** are illustrated in Scheme 1. Briefly, ethyl bromoacetate **1** was substituted with sodium thiosulfate to form the Bunte salt ethyl acetate-2-sodium thiosulfate **2**, followed by substitution at the 3-position of indole (or substituted indole) and hydrolysis to yield a key intermediate **5**. Finally, this intermediate was coupled with different substituted benzylamines to afford the target products **6a-d**. Compound **6c9** was also generated via Suzuki-Miyaura cross-coupling of **6c8** with phenylboronic acid. All the target compounds were obtained in high purity (>95%) via separation using a flash column. They were fully characterized through NMR and high-resolution mass spectrometry. Details of the chemical synthesis and structural characterization can be found in the Materials and Experimental Details section. The ^1H and ^{13}C NMR spectra of **6a-d** are presented in the supplementary material.

2.1. Design, synthesis, and structure-activity relationship research of compounds **6a1-6**, **6b1-7**, and **6c1-8**

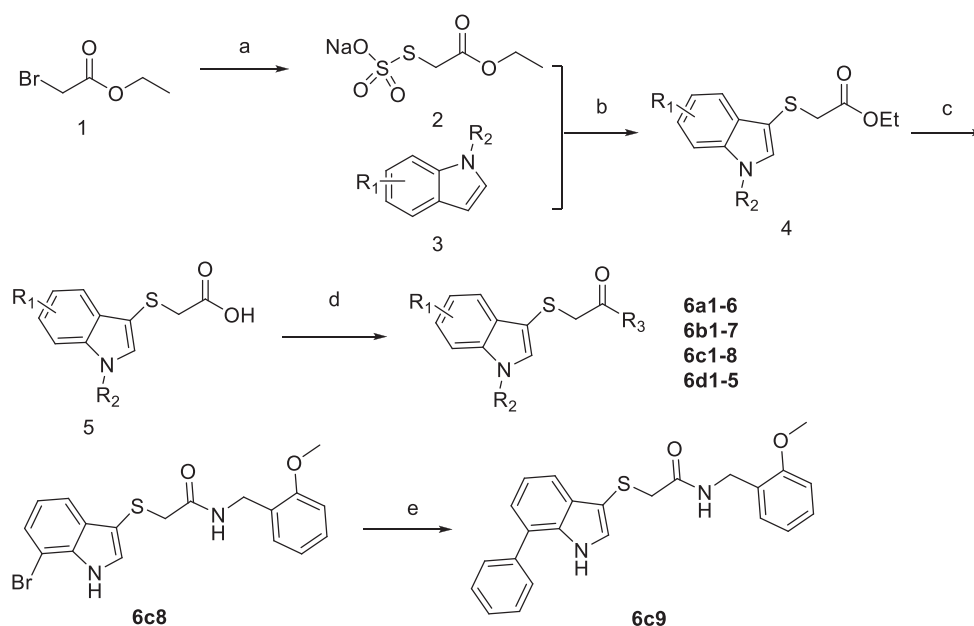
In our previous work, we discovered that 2-((1*H*-indol-3-yl)thio)-*N*-phenyl-acetamide specifically targets the RdRp of both RSV and IAV, resulting in replication inhibition at sub-micromolar EC_{50}

values [35,36]. After the outbreak of COVID-19, we screened these compounds and found that several 2-((indol-3-yl)thio) acetamides moderately inhibited SARS-CoV-2 RdRp at $10 \mu\text{M}$. When substituted aniline, at the right part of the molecule, was replaced with a benzylaniline, increased potency of the compounds was observed (Fig. 2). Thus, a new series of 2-((indol-3-yl)thio)-*N*-benzyl-acetamides was designed. Compounds **6a1-6**, **6b1-7**, and **6c1-8** were prepared via the substitution of ethyl acetate-2-sodium thiosulfate with indole (or methyl-/bromo-substituted indole), followed by hydrolysis and coupling with a series of benzylamines.

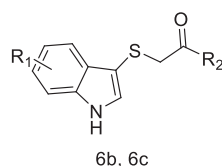
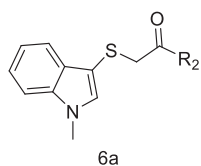
Subsequently, these compounds were tested for their SARS-CoV-2 RdRp inhibitory effect in a Gluc reporter system specifically initiated by the coronavirus RdRp, utilizing remdesivir as the positive control. The IC_{50} values of compounds **6a1-6**, **6b1-7**, and **6c1-8** against SARS-CoV-2 RdRp are listed in Table 1. The cytotoxicity of these compounds was also tested under the same conditions.

As shown in Table 1, five out of the six compounds in the series **6a1-6** showed moderate SARS-CoV-2 RdRp inhibitory activity (45%–76%) at $10 \mu\text{M}$, and the IC_{50} value of the most potent compound **6a6** was measured to be $7.50 \pm 1.68 \mu\text{M}$. Compound **6a1** was the simplest in the series and showed moderate inhibitory activity. After the introduction of another benzyl group to the nitrogen atom in the amide, the RdRp inhibitory activity was enhanced, as shown by the IC_{50} values of **6a1** ($26.92 \mu\text{M}$) vs. **6a2** ($12.30 \mu\text{M}$). However, after introducing an electron-withdrawing trifluoromethyl group at the 4-position of the benzyl ring, the activity was completely lost (**6a3** vs. **6a1**). The substitution with *O*-alkylated groups (e.g., methoxyl and dimethylaminoethoxy) or chlorine atom on the benzyl ring is also beneficial for the SARS-CoV-2 RdRp inhibitory effect (**6a4-6** vs. **6a1**).

When the starting material *N*-methyl indole was replaced by indole, compounds in the series **6b1-7** were obtained. After the removal of the *N*-methyl group, the RdRp inhibitory activity significantly increased; compounds **6b1-2** were four times more potent than **6a1-2**, as indicated by their IC_{50} values. Similar to **6a3**, **6b3** exhibited a significantly high inhibitory effect. These results

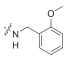
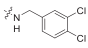


Scheme 1. General synthetic scheme for compounds **6a-d**. Reagents and conditions: (a) $\text{Na}_2\text{S}_2\text{O}_3$, $\text{MeOH}/\text{H}_2\text{O}$; (b) Iodine, DMSO, 60°C ; (c) NaOH , $\text{EtOH}/\text{H}_2\text{O}$; (d) HATU, DIEA, dichloromethane; (e) Phenylboronic acid, $\text{Pd}_2(\text{dba})_3$, Sphos, cesium Carbonate, 1,4-dioxane.

Table 1Structure, log P value, and SARS-CoV-2 RdRp inhibitory activity of compounds **6a1-6**, **6b1-6**, and **6c1-8**.

Compounds	R ₁	R ₂	Log P ^a	Anti-SARS-CoV-2 RdRp IC ₅₀ (μM)	CC ₅₀ (μM) ^b
6a1	- ^b		3.09	26.92 ± 3.54	95.50
6a2	- ^b		4.74	12.3 ± 1.40	91.20
6a3	- ^b		3.99	NA ^c	>100
6a4	- ^b		3.18	8.91 ± 0.87	>100
6a5	- ^b		3.10	9.82 ± 0.96	>100
6a6	- ^b		4.38	7.50 ± 1.68	>100
6b1	H		3.03	6.81 ± 1.03	>100
6b2	H		4.67	3.35 ± 0.21	>100
6b3	H		3.92	7.94 ± 1.02	>100
6b4	H		3.11	9.08 ± 1.38	>100
6b5	H		3.27	4.55 ± 0.23	>100
6b6	H		3.28	7.64 ± 0.54	>100
6b7	H		3.58	6.68 ± 0.86	>100
6c1	4-Br		3.80	8.71 ± 0.33	>100
6c2	4-Br		5.07	7.21 ± 0.59	>100
6c3	5-Br		3.82	10.72 ± 1.11	>100
6c4	5-Br		5.09	9.77 ± 0.46	>100
6c5	6-Br		3.82	10.01 ± 0.95	>100
6c6	6-Br		5.09	8.71 ± 0.63	67.61

Table 1 (continued)

Compounds	R ₁	R ₂	Log P ^a	Anti-SARS-CoV-2 RdRp IC ₅₀ (μM)	CC ₅₀ (μM) ^b
6c7	7-Br		3.80	7.08 ± 0.65	72.44
6c8	7-Br		5.07	4.55 ± 0.25	>100
Remdesivir	—	—	2.82	1.56 ± 0.12	>100

All data are expressed as mean ± SD of triplicate assays.

^a Log P = Predicted octanol/water partition coefficient. The log P values were predicted using molinspiration (<https://www.molinspiration.com/services/logp.html>).

^b The half-maximal cytotoxic concentration (CC₅₀) for each compound was calculated by comparing the viability of compounds-treated cells with that of DMSO-treated cells in cell countingkit-8 (CCK-8) assay.

^c NA: not active.

indicate that the -NH- fragment is beneficial to their SARS-CoV-2 RdRp inhibitory activity, and this may be attributed to a hydrogen bond interaction between the ligand and receptor. Furthermore, the addition of another methyl or benzyl group at the nitrogen atom of amide slightly enhanced SARS-CoV-2 RdRp inhibitory activity, as indicated by the IC₅₀ values of **6b1** (6.81 μM) vs. **6b2** (3.31 μM) or **6b5** (4.55 μM). Meanwhile, a methyl group introduced to the methylene group of benzylamine caused negligible effects on SARS-CoV-2 RdRp inhibitory activity, as evidenced by the IC₅₀ values of **6b1** (6.81 μM) and **6b7** (6.68 μM).

In our previous study [35], we found that a bromine atom introduced on the indole ring can significantly increase the RdRp inhibitory effects of compounds in this series against IAV and RSV; thus, derivatives with a bromine substitution (**6c1-8**) were also designed and synthesized. All of these compounds exhibited potent inhibitory effects, and their IC₅₀ values were in the range of 4.55–10.72 μM. Among these brominated compounds, **6c1-2** and **6c7-8** displayed a more potent RdRp inhibitory activity than **6c3-6**, suggesting that bromine substitution at position 4- or 7- is highly suitable for their interaction with RdRp.

2.2. Design, synthesis, and SAR research of compounds **6c9** and **6d1-5**

To obtain highly efficacious SARS-CoV-2 RdRp inhibitors, compounds **6d1-5** were designed and synthesized using 4-/7-brominated indole and substituted benzylamine as the starting materials in the second-round optimization. Meanwhile, **6c9** was also synthesized to confirm whether another conjugation of benzene ring with indole benefits RdRp inhibition.

After the synthesis of these derivatives, their SARS-CoV-2 RdRp inhibition activities were assayed as described above. As listed in Table 2 and depicted in Fig. 3, **6c9** shows significantly increased SARS-CoV-2 RdRp inhibitory activity (IC₅₀ = 1.65 ± 0.05 μM), indicating that it could act as a lead compound for the development of a novel SARS-CoV-2 RdRp inhibitor with high potency and improved drug-likeness properties. Derivatives **6d1-4** were designed based on the SAR obtained in the first-round optimization, and most of them exhibited good activities except **6d3**. These results also proved that di-substitution on the amide nitrogen atom is beneficial for RdRp inhibition. To improve the drug-likeness properties of **6d1-2**, another oxygen atom and ethoxyl were introduced into the molecule and thus compound **6d5** was obtained. Notably, it was identified as the most potent SARS-CoV-2 RdRp inhibitor with an IC₅₀ value of 1.11 ± 0.05 μM and an acceptable log P value of 4.38.

As illustrated in Fig. 3, all the selected compounds **6b2**, **6b5**, **6c9**, **6d2**, and **6d5** showed dose-dependent inhibition of SARS-CoV-2 RdRp, and the activity was comparable to that of remdesivir, as indicated by the IC₅₀ values. Compound **6d5** was identified as the

most promising candidate with a lower IC₅₀ value than remdesivir and an excellent safety index.

2.3. Compounds **6b2**, **6b5**, **6c9**, **6d2**, and **6d5** inhibit RNA synthesis by SARS-CoV-2 RdRp

After identifying the most potent SARS-CoV-2 RdRp inhibitors in the CoV-RdRp-Gluc reporter assay, we decided to evaluate whether they could also inhibit the efficiency of RNA synthesis by SARS-CoV-2 RdRp. Treatment with 5 μM and 10 μM of the compounds **6b2**, **6b5**, **6c9**, **6d2**, **6d5**, or remdesivir decreased the levels of viral plus- and minus-strand Gluc RNA in a dose-dependent manner (Fig. 4A–F). Compounds **6b5**, **6c9**, and **6d5** diminished the levels of both plus- and minus-strand Gluc RNA more potently than the positive control (remdesivir). These data confirm that **6b2**, **6b5**, **6c9**, **6d2**, and **6d5** act as SARS-CoV-2 RdRp inhibitors.

2.4. **6b2**, **6b5**, **6c9**, **6d2**, and **6d5** are resistant to proofreading activity of nsp14/nsp10

Coronavirus nonstructural protein 14 (nsp14) exoribonuclease in complex with its activator nonstructural protein 10 (nsp10) performs a proofreading function during coronavirus replication. It can excise erroneous mutagenic nucleotides incorporated by nsp12 into viral RNA. Ribavirin was reported to be excised from the nascent RNA strand of CoVs and showed limited efficacy in vivo [37]. To confirm whether compounds **6b2**, **6b5**, **6c9**, **6d2**, and **6d5** are resistant to the proofreading activity of exoribonuclease, we co-expressed nsp14 and nsp10 into the cell-based CoV-RdRp-Gluc system. Gluc activity of these compounds slightly declined in the presence of nsp14 and nsp10. All the compounds tested showed good tolerance of nps14/nsp10 with slightly increased IC₅₀ values (Fig. 5 and Table 3), when compared with the data in Fig. 4. The IC₅₀ values for **6b2**, **6b5**, **6c9**, **6d2**, and **6d5** increased to a lesser extent than that of remdesivir, indicating that these compounds are more tolerant to CoV exoribonuclease. Compounds **6c9** and **6d5** were identified as the most promising inhibitors against SARS-CoV-2 RdRp; their IC₅₀ values were 2.18 μM and 1.89 μM, respectively, in the presence of nsp10/nsp14 exoribonuclease.

In our previous study [38], we suggested that nsp10/nsp14 exoribonuclease must be included in the cell-based CoV-RdRp-Gluc assay to identify effective RdRp inhibitors, as the exoribonuclease complex nsp14/nsp10 renders SARS-CoV-2 RdRp resistant to NA inhibitors. Ribavirin can be excised by exoribonuclease from the nascent RNA strand of CoVs to diminish its antiviral effect. Compounds **6b2**, **6b5**, **6c9**, **6d2**, and **6d5** showed better tolerance to nps14/nsp10 than remdesivir, indicating that these compounds may be more potent inhibitors of SARS-CoV-2 than remdesivir.

Table 2
Structure, log P value, and SARS-CoV-2 RdRp inhibitory activity of compounds **6c9** and **6d1-5**.

Compounds	R ₁	R ₂	Log P ^a	Anti-SARS-CoV-2 RdRp IC ₅₀ (μM)	CC ₅₀ (μM) ^b
6c9	7-Ph		4.78	1.65 ± 0.05	95.52 ± 3.11
6d1	4-Br		4.03	4.73 ± 0.67	25.12
6d2	4-Br		5.43	3.76 ± 0.79	25.7
6d3	7-Br		4.03	20.89 ± 2.68	52.48
6d4	7-Br		5.43	7.08 ± 0.32	>100
6d5	4-Br		4.38	1.11 ± 0.05	>100
Remdesivir	—	—	2.82	1.19 ± 0.36	>100

All data are expressed as mean ± SD of triplicate assays.

^a Log P = Predicted octanol/water partition coefficient. The log P values were predicted using molinspiration (<https://www.molinspiration.com/services/logp.html>).

^b The half-maximal cytotoxic concentration (CC₅₀) for each compound was calculated by comparing the viability of compounds-treated cells with that of DMSO-treated cells in cell countingkit-8 (CCK-8, Beyotime) assay.

2.5. Evaluation of antiviral activity of **6d5** against HCoV-OC43 and HCoV-NL63

Compound **6d5** was selected for evaluation of its antiviral effect against the human coronavirus strains HCoV-OC43 and HCoV-NL63, which are commonly used in antiviral drug screening, in a cell-based assay *in vitro*. The data in Fig. 6 illustrate that replication of HCoV-OC43 and HCoV-NL63 was effectively inhibited in a dose-dependent manner after treatment with serially diluted **6d5**. In particular, **6d5** showed a more potent inhibitory effect than remdesivir on HCoV-OC43 replication. Moreover, **6d5** exhibited a higher antiviral activity against HCoV-OC43 (which belongs to the same β-coronavirus as SARS-CoV-2) than against HCoV-NL63 (an α-coronavirus).

According to serology studies and genomic analysis, coronavirus is divided into four genera: α-coronavirus, β-coronavirus, γ-coronavirus, and δ-coronavirus. HCoV-OC43 and SARS-CoV-2 are members of the β-coronavirus, whereas HCoV-NL63 is a member of the α-coronavirus. The higher antiviral activity of **6d5** against HCoV-OC43 than against HCoV-NL63 implies that this compound may act as a potent SARS-CoV-2 inhibitor.

2.6. Molecular modeling studies

To explore the binding mode of identified inhibitors, molecular docking study of the most potent compound **6d5** against SARS-CoV-2 RdRp (PDB-ID: 6M7K) was performed using AutoDock Vina.

As shown in Fig. 7, the binding pocket of **6d5** is located in the

palm and finger subdomains of SARS-CoV-2 RdRp. The hydrogen on the indole nitrogen of **6d5** formed strong hydrogen bonds with Asp760, a highly conserved catalytic residue that is required for RNA synthesis. An H-bond interaction between the carbonyl oxygen atoms of **6d5** and Cys622 was also observed. Moreover, the benzene ring in 2-ethoxyaniline formed a π-cation and an edge-to-face π-π interaction with residues Arg553 and Try445, respectively.

To gain further insight into the structure-activity relationships of the **6d5** analogs, five 2-((1H-indol-3-yl)thio)-N-benzyl-acetamide derivatives (**6a1**, **6a2**, **6b2**, **6c7**, and **6c9**) that exhibited diverse inhibitory activities were also docked to SARS-CoV-2 RdRp. The calculated binding energies (DG_{ADV}) and predicted binding poses of these derivatives are depicted in Fig. 8 and Fig. 9, respectively. The values of DG_{ADV} were used to estimate the relative binding affinity of the inhibitors. As seen in Fig. 8, there is a positive linear relationship between DG_{ADV} of selected derivatives and their corresponding experimental IC₅₀ values against SARS-CoV-2 RdRp (R² = 0.83), implying that the strong inhibitory effect of compounds is associated with their high binding affinity to SARS-CoV-2 RdRp. In addition, because of their common structural skeleton, it is reasonable to assume that the binding sites of these derivatives are similar to those of **6d5**. As expected, all compounds presented a similar arrangement within the central cavity of SARS-CoV-2 RdRp (Fig. 9A).

Comparison of 6a1 and 6a2. As the simplest compound in the series, **6a1** showed a moderate binding energy (−5.0 kcal/mol). After the introduction of another benzyl group to the nitrogen atom in the amide, a more favorable binding energy was obtained for **6a2**

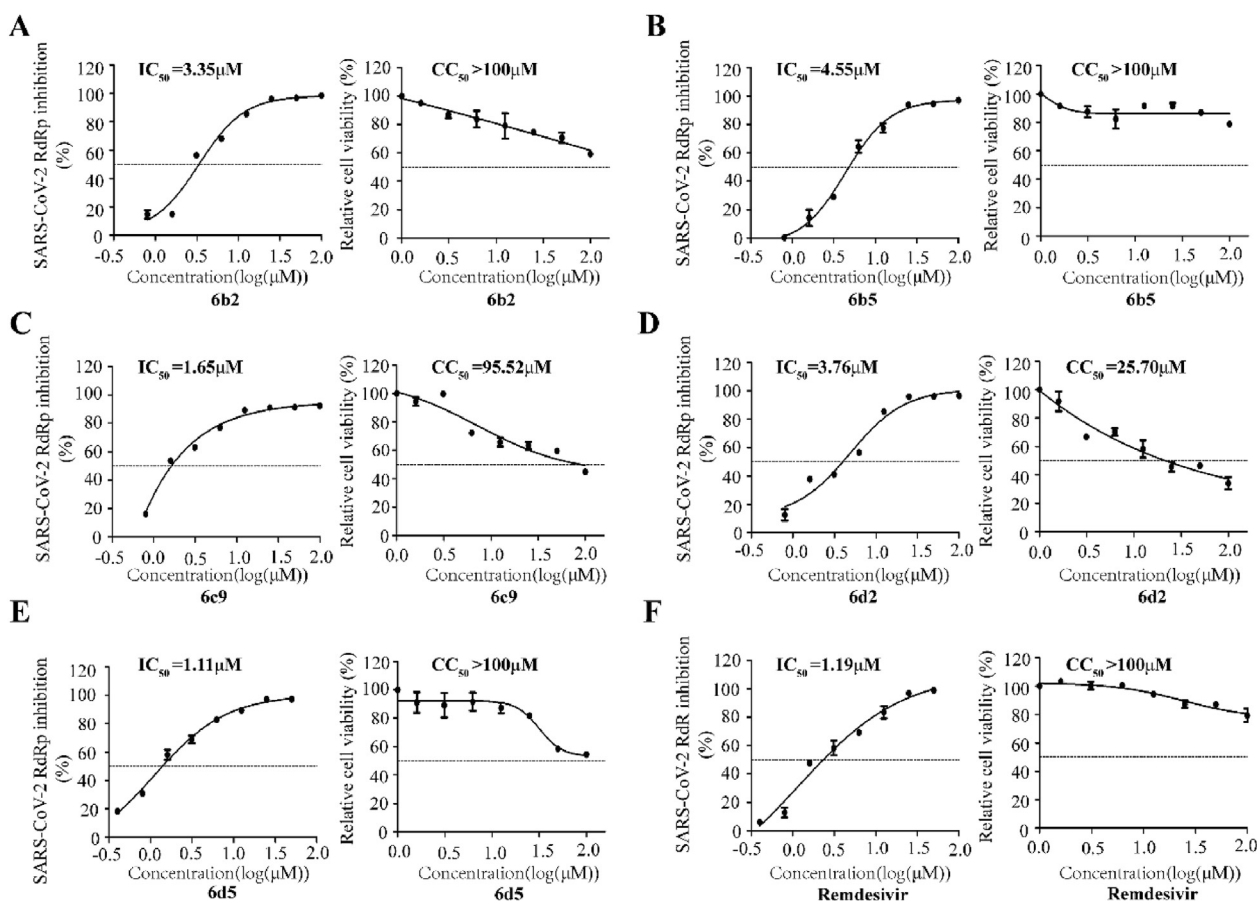


Fig. 3. Dose-response inhibition curves of selected compounds **6b2**, **6b5**, **6c9**, **6d2**, and **6d5** against SARS-CoV-2 RdRp. HEK293T cells were transfected with CoV-Gluc, nsp12, nsp7, and nsp8 plasmid DNA at the ratio of 1:10:30:30. At 12 h post-transfection, the cells were re-seeded in 96-well plates (10^4 /well) and treated with serially diluted compounds **6b2** (A), **6b5** (B), **6c9** (C), **6d2** (D), **6d5** (E) and remdesivir (F). Gluc activity in the supernatants was measured. CC_{50} values in the cells were measured using CCK-8 kits. All data are expressed as mean \pm SD of triplicate assays.

(-6.1 kcal/mol). Although the H-bond interactions were lost, the benzene ring of **6a2** contributed to additional hydrophobic interactions with Phe793 and Met794. Additionally, strong π -cation interactions were observed between **6a2** and Arg553. These observations may explain why **6a2** had a stronger inhibitory effect than **6a1**.

Comparison of 6b2 and 6a2. The calculated binding energy of **6b2** was -7.1 kcal/mol, which is more favorable than that of **6a2**. The only structural difference between **6a2** and **6b2** is the substituent at the nitrogen atom of indole. As seen in Fig. 9C, there is an additional H-bond between the $-NH-$ fragment in the indole ring and the carboxyl group of Asp623 and may account for the stronger inhibitory activity of **6b2** ($IC_{50} = 3.35 \mu M$) than that of **6a2**.

Comparison of 6c7 and 6c9. The only structural difference between **6c7** and **6c9** is the substituent on the benzene ring of indole. When the bromine atom in **6c7** was replaced with a benzene ring, additional hydrophobic interactions were formed between **6c9** and palm subdomain residues Try800, Phe812, and Cys813. Consequently, **6c9** exhibited more favorable binding energy (-7.2 kcal/mol) than **6c7** (-6.1 kcal/mol). Thus, we speculated that the introduction of a benzene ring at this position improves the inhibitory effect of the compounds.

3. Conclusion

RdRp is a crucial enzyme in the life cycle of most RNA viruses. Considering that this enzyme has no human counterpart and that it

is essential for the life cycle of viruses, it is a popular therapeutic drug target pursued by pharmaceutical companies and academic research groups. RdRp is considered a conserved protein within RNA viruses; thus, scientists worldwide have repurposed pre-existing drugs that target RdRp to identify candidates against SARS-CoV-2. In this paper, we report the discovery of SARS-CoV-2 RdRp inhibitors based on the structural optimization of the IAV and RSV RdRp ligands. After a two-round optimization, compounds **6b2**, **6b5**, **6c9**, **6d2**, and **6d5** were identified as potent RdRp inhibitors with IC_{50} values of $3.35 \pm 0.21 \mu M$, $4.55 \pm 0.2 \mu M$, $1.65 \pm 0.05 \mu M$, $3.76 \pm 0.79 \mu M$, and $1.11 \pm 0.05 \mu M$, respectively, whereas the IC_{50} of remdesivir (control) was measured as $1.19 \pm 0.36 \mu M$. Compound **6d5** was identified as the most potent candidate, having a more potent inhibitory activity than remdesivir against HCoV-OC43 in a cell-based assay.

Molecular docking studies were carried out to explore the binding mode and structure-activity relationships of 2-((1H-indol-3-yl)thio)-N-benzyl-acetamide derivatives. As seen in Figs. 7A and 9A, the predicted binding sites of these inhibitors were located at the palm and finger subdomains of SARS-CoV-2 RdRp. Specifically, these active compounds interact with motif A residues D618-R624, palm domain residues K794, S795, D760, and D761, and finger domain residues D452, Y455, K551, and R553. Given that D618, D760, and D761 are involved in binding two magnesium ions at the catalytic center, the binding of these compounds may block the conformational change required to coordinate the divalent cations during the catalytic process. Notably, the strong correlation

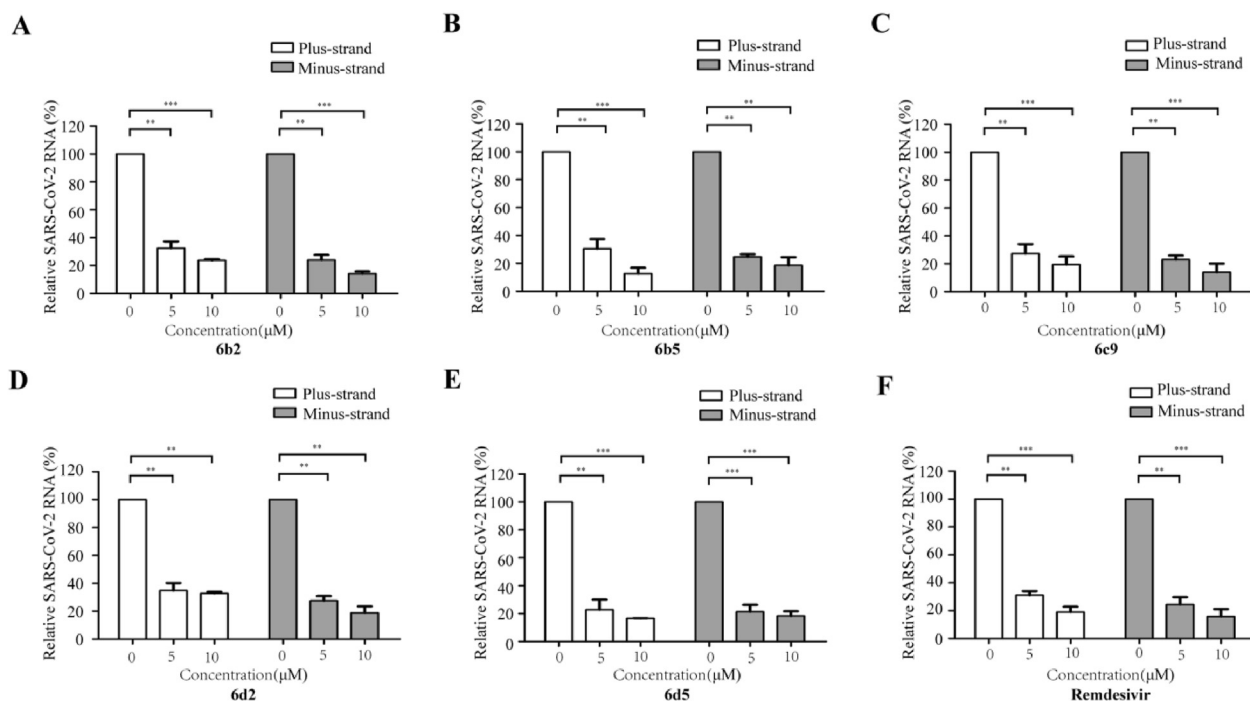


Fig. 4. Inhibition of CoV-Gluc RNA expression by 6b2, 6b5, 6c9, 6d2, and 6d5. HEK293T cells were transfected with CoV-Gluc, nsp12, nsp7, and nsp8 plasmid DNA at the ratio of 1:10:30:30. At 6 h post-transfection, supernatants were replaced with fresh medium containing 6b2 (A), 6b5 (B), 6c9 (C), 6d2 (D), 6d5 (E), and remdesivir (F). The cells were cultured for additional 24 h, total cellular RNA was extracted, and CoV-Gluc levels were determined via real-time qRT-PCR. Error bars indicate SD, **p < 0.01, ***p < 0.001.

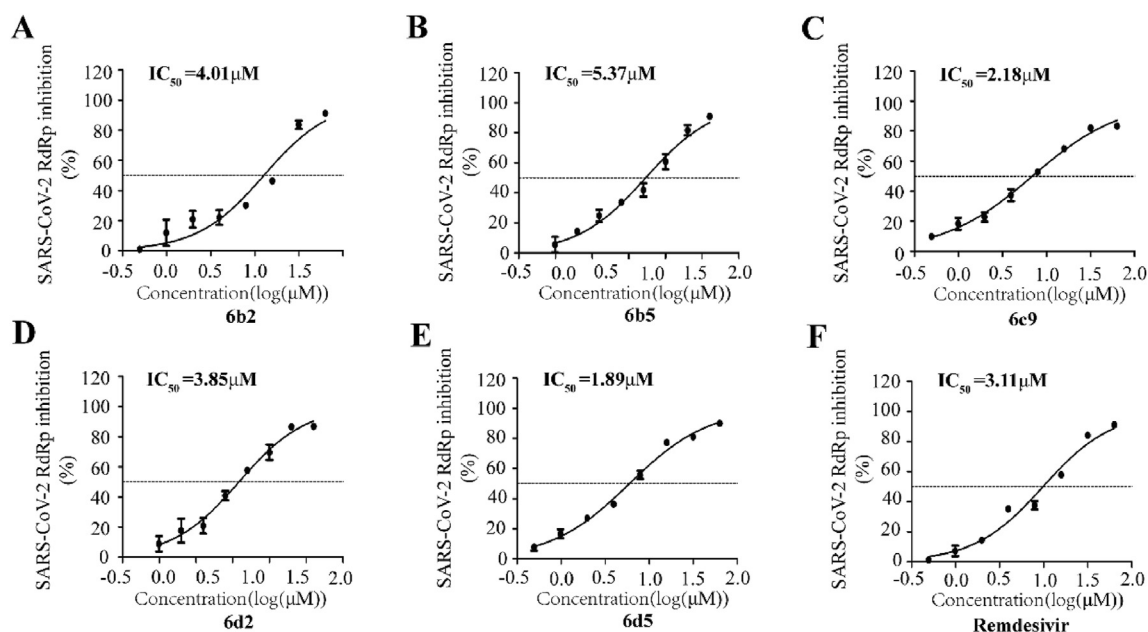


Fig. 5. 6b2, 6b5, 6c9, 6d2, and 6d5 were resistant to the proofreading activity of nsp14/nsp10. HEK293T cells were co-transfected with CoV-Gluc, nsp7, nsp8, nsp10, and nsp14 plasmids at a ratio of 1:10:30:30:25:25. Gluc activity was determined using a cell-based assay. The IC_{50} values of 6b2 (A), 6b5 (B), 6c9 (C), 6d2 (D), 6d5 (E), and remdesivir (F) were determined using a cell-based system with the nsp10/nsp14 proofreading function.

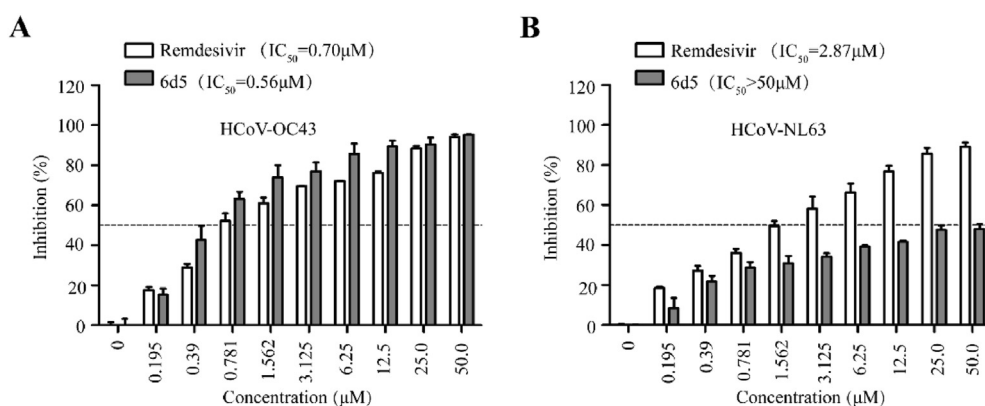
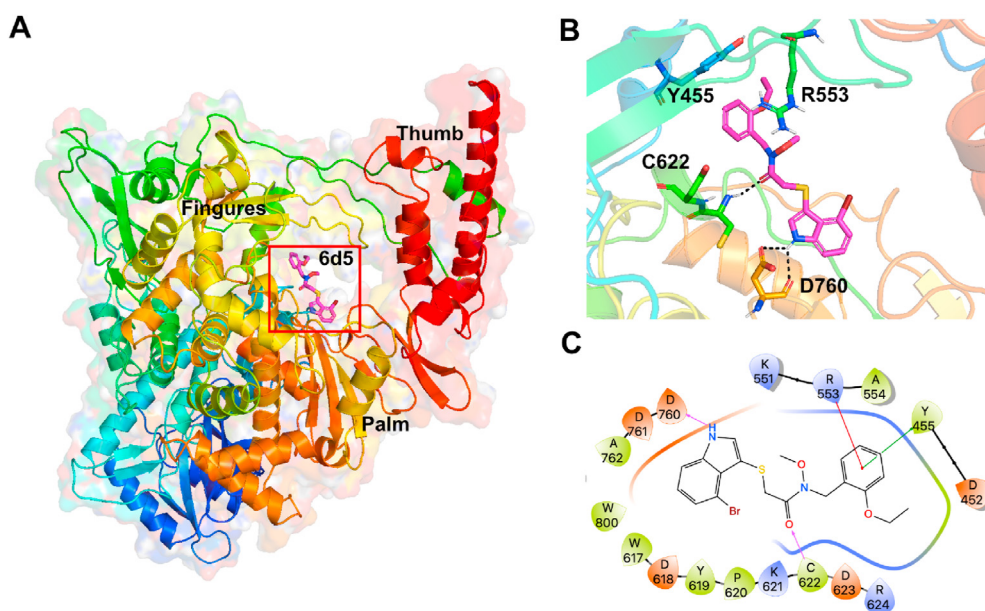
between the calculated binding energies and experimental IC_{50} values implies that the strong inhibitory effect of compounds is associated with their high binding affinity to SARS-CoV-2 RdRp. Structure-activity relationship analysis highlighted that the -NH-fragment in the indole ring makes an important contribution to the binding of RdRp through a hydrogen bond and that an additional aromatic ring on the indole ring or the nitrogen in amide is

beneficial for the ligand-receptor interaction.

We often believe that drugs should be of nanomolar potency in medicinal chemistry, and most approved drugs comply with this “nanomolar rule”; however, there are a few exceptions such as sofosbuvir, favipiravir, and ribavirin. Thus, further structural optimization for the improvement of the activity is underway. The current work is a successful attempt to identify new anti-SARS-

Table 3IC₅₀ values of **6b2**, **6b5**, **6c9**, **6d2**, and **6d5** for SARS-CoV-2 RdRp inhibitory activity with or without nsp14/nsp10.

Compounds	Nsp12 (IC ₅₀ /μM) ^a	Nsp12 + 14/10 (IC ₅₀ /μM) ^b	Ratio ((12 + 14/10)/12)
6b2	3.35	4.01	1.20
6b5	4.55	5.37	1.18
6c9	1.65	2.18	1.32
6d2	3.76	3.85	1.02
6d5	1.11	1.89	1.70
Remdesivir	1.19	3.11	2.61

^a IC₅₀ values of **6b2**, **6b5**, **6c9**, **6d2**, and **6d5** against SARS-CoV-2 RdRp without nsp14/nsp10 exoribonuclease.^b IC₅₀ values of **6b2**, **6b5**, **6c9**, **6d2**, and **6d5** against SARS-CoV-2 RdRp with nsp14/nsp10 exoribonuclease.**Fig. 6.** Evaluation of antiviral activity of **6d5** against human coronavirus strains HCoV-OC43 and HCoV-NL63. HCT-8 and LLC-MK2 cells were infected by HCoV-OC43 (A) or HCoV-NL63 (B) at a MOI (multiplicity of infection) of 0.1 and 0.01, respectively, and treated with serial dilutions of **6d5** and remdesivir at 1 h post-infection. The effect of the treatments on cell viability was measured via MTS assay at 120 h post-infection.**Fig. 7.** Binding pose analysis of compound **6d5**. (A) Predicted structure of SARS-CoV-2 RdRp in complex with compound **6d5**. (B) Key interactions between compound **6d5** and SARS-CoV-2 RdRp. (C) Residues within 5 Å of compound **6d5** are shown on the 2D ligand interaction diagram. For clarity, only polar hydrogen atoms are shown. Dark blue, red, and green indicate positively charged, negatively charged, and hydrophobic residues, respectively. Hydrogen bonding is depicted as magenta arrows, π -cation interactions are depicted as red lines, and π - π interactions are depicted as green lines.

CoV-2 candidates from other viral RdRp inhibitors.

In summary, a new series of 2-((indol-3-yl)thio)-N-benzylacetamides was designed and synthesized based on the screening results of our antiviral library and a two-round optimization, and **6b2**, **6b5**, **6c9**, **6d2**, and **6d5** were identified as potent SARS-CoV-2

RdRp inhibitors. They can inhibit the efficiency of RNA synthesis by SARS-CoV-2 RdRp and diminish the level of both plus- and minus-strand Gluc RNA more potently than the positive control remdesivir. The most potent compound **6d5** showed stronger inhibitory activity than remdesivir against HCoV-OC43 in cells and has been

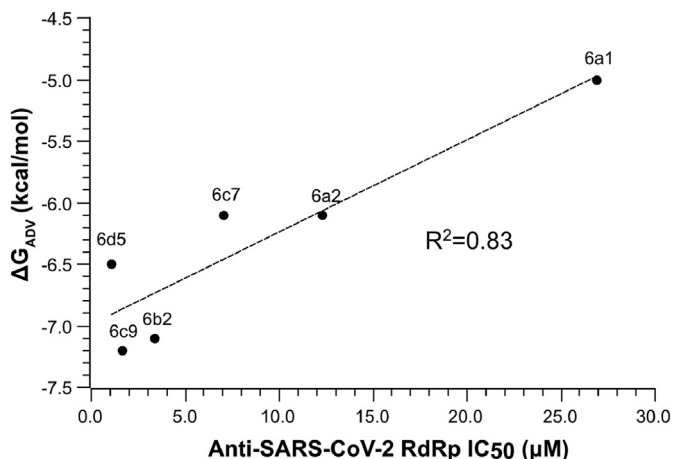


Fig. 8. Correlation of calculated binding energies of selected compounds with their corresponding experimental IC_{50} values against SARS-CoV-2 RdRp.

selected as a potential candidate for further investigation.

4. Materials and experimental details

4.1. Chemicals and instruments

All starting materials for chemical synthesis were purchased from commercial suppliers (Shanghai Bide Pharmaceutical Technology Co., Ltd. & Beijing InnoChem Science & Technology Co., Ltd) and used without further purification. NMR spectra were recorded on Bruker Avance 400 MHz and 500 MHz spectrometers. LC-MS and purity data were measured using an Agilent HPLC/MSD instrument. APCI high-resolution mass spectra (HRMS) were recorded on an Autospec Ultima-TOF spectrometer.

4.2. Synthesis

4.2.1. Sodium S-(2-ethoxy-2-oxoethyl) sulfurothioate **2**

To a solution of ethyl bromoacetate (5.5 mL, 50 mmol) in 75 mL of methanol and 25 mL of H_2O , sodium thiosulfate pentahydrate (14.88g, 60 mmol) was added and the solution was stirred for 1h at 65 °C. The solvent was evaporated under reduced pressure, and 50 mL of methanol and 50 mL of dichloromethane were added. The mixture was washed with ultrasonic for 5 min and filtered with suction. After concentration under reduced pressure, 10.86 g of sodium S-(2-ethoxy-2-oxoethyl) sulfurothioate **2** was obtained as a light-yellow solid which was used directly for the next step.

1H NMR (400 MHz, Methanol- d_4) δ 4.19 (q, J = 7.1 Hz, 2H), 3.84 (s, 2H), 1.28 (t, J = 7.1 Hz, 3H). ^{13}C NMR (101 MHz, Methanol- d_4) δ 62.8, 37.5, 14.4. ESI-MS(m/z): 220.8 [$M - Na$].

4.2.2. General procedure for the synthesis of **5a-f**

To a solution of indole/substituted indole (49 mmol) and Sodium S-(2-ethoxy-2-oxoethyl) sulfurothioate **2** (10.86g, 49 mmol) in DMSO, iodine (1.42g, 5.6 mmol) was added. The solution was stirred for 30min at 60 °C and 200 mL of ethyl acetate was added after the solution was cooled to 30 °C. the mixture was washed with 100 mL of saturated sodium thiosulfate, 1000 mL of water, and 100 mL of saturated saline the organic phase was dried over anhydrous sodium sulfate and concentrated under reduced pressure. After purification on a silica column compounds **4a-f** was afforded.

To a solution of compounds **4a** (5.31g, 25.62 mmol) in MeOH and H_2O (24 mL + 6 mL), sodium hydroxide (1.23g, 30.75 mmol) was added. The solution was stirred for 30min at 25 °C and extracted with ether. The pH of aqueous phase was adjusted to 3–4 and extracted with ethyl acetate (50 mL x 3). After removal of the solvent under reduced pressure **5a** was afforded (quantitative). The synthesis of **5b-f** was similar to that of **5a**.

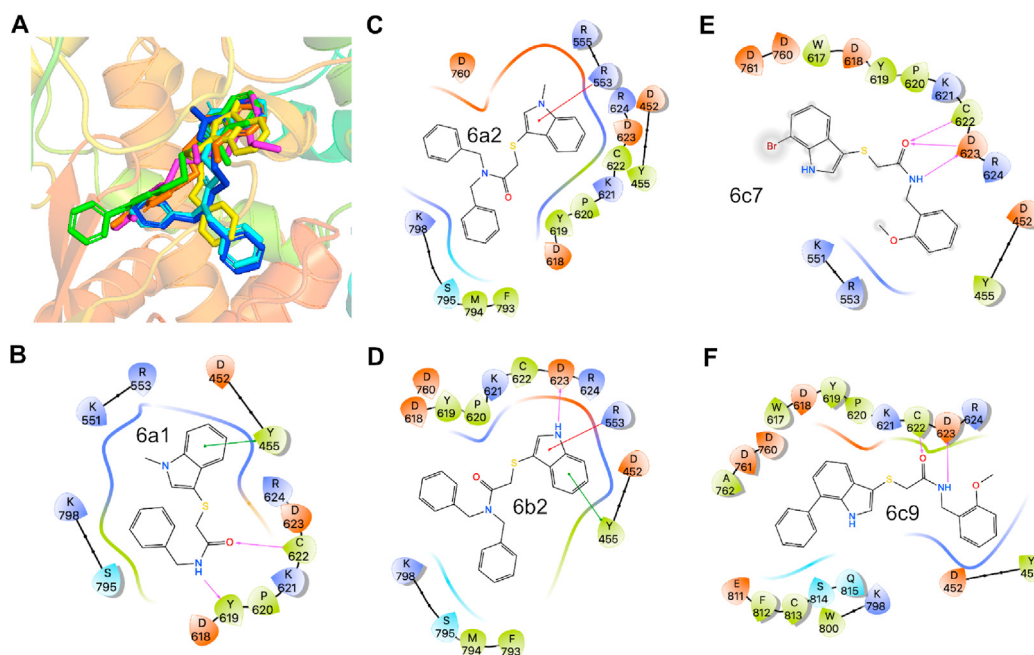


Fig. 9. Predicted binding poses for five 2-((1H-indol-3-yl)thio)-N-benzyl-acetamides derivatives. (A) Superposition of binding sites of selected compounds. Color codes: **6a1** (yellow), **6a2** (blue), **6b2** (cyan), **6c7** (orange), **6c9** (green), and **6d5** (purple). (B–G) The 2D ligand interaction diagrams for selected compounds. For clarity, only polar hydrogen atoms are shown. Dark blue, red, cyan and green indicate positively charged, negatively charged, polar, and hydrophobic residues, respectively. Hydrogen bonding is depicted as magenta arrows, π -cation interactions are depicted as red lines, and π - π interactions are depicted as green lines.

4.2.3. 2-((1-Methyl-1H-indol-3-yl)thio)acetic acid **5a**

^1H NMR (500 MHz, DMSO- d_6) δ 12.48 (s, 1H), 7.64 (d, J = 7.9 Hz, 1H), 7.54 (s, 1H), 7.47 (d, J = 8.2 Hz, 1H), 7.22 (t, J = 7.6 Hz, 1H), 7.14 (t, J = 7.5 Hz, 1H), 3.78 (s, 3H), 3.38 (s, 2H). ^{13}C NMR (126 MHz, DMSO- d_6) δ 171.7, 137.3, 135.3, 129.6, 122.4, 120.3, 119.1, 110.8, 101.9, 39.4, 33.1. ESI-MS (m/z): 220.2 [$\text{M} - \text{H}$] $^-$.

4.2.4. 2-((1H-indol-3-yl)thio)acetic acid **5b**

^1H NMR (400 MHz, DMSO- d_6) δ 11.41 (s, 2H), 7.62 (dd, J = 7.8, 1.1 Hz, 2H), 7.52 (d, J = 2.6 Hz, 2H), 7.41 (dt, J = 8.1, 0.9 Hz, 2H), 7.15 (ddd, J = 8.1, 7.0, 1.4 Hz, 2H), 7.09 (ddd, J = 8.0, 7.0, 1.2 Hz, 2H), 2.50 (p, J = 1.8 Hz, 2H). ^{13}C NMR (101 MHz, DMSO- d_6) δ 171.23, 136.27, 130.92, 128.70, 121.79, 119.66, 118.40, 112.05, 102.37, 38.77. ESI-MS (m/z): 206.2 [$\text{M} - \text{H}$] $^-$.

4.2.5. 2-((4-Bromo-1H-indol-3-yl)thio)acetic acid **5c**

^1H NMR (500 MHz, DMSO- d_6) δ 12.43 (s, 0H), 11.73 (s, 1H), 7.58 (d, J = 2.6 Hz, 1H), 7.45 (d, J = 8.1 Hz, 1H), 7.27 (d, J = 7.5 Hz, 1H), 7.05 (t, J = 7.8 Hz, 1H), 3.47 (s, 2H). ^{13}C NMR (126 MHz, DMSO- d_6) δ 171.1, 138.3, 133.6, 125.8, 124.7, 123.5, 113.3, 112.5, 103.3, 40.9. ESI-MS (m/z): 284.1 [$\text{M} - \text{H}$] $^-$.

4.2.6. 2-((5-Bromo-1H-indol-3-yl)thio)acetic acid **5d**

^1H NMR (500 MHz, DMSO- d_6) δ 12.49 (s, 1H), 11.65 (s, 1H), 7.79 (d, J = 2.0 Hz, 1H), 7.63 (d, J = 2.6 Hz, 1H), 7.42 (d, J = 8.6 Hz, 1H), 7.29 (dd, J = 8.6, 1.9 Hz, 1H), 3.41 (s, 2H). ^{13}C NMR (126 MHz, DMSO- d_6) δ 171.7, 135.5, 133.2, 131.2, 124.9, 121.2, 114.6, 113.0, 102.7, 39.3. ESI-MS (m/z): 284.1 [$\text{M} - \text{H}$] $^-$.

4.2.7. 2-((6-Bromo-1H-indol-3-yl)thio)acetic acid **5e**

^1H NMR (500 MHz, DMSO- d_6) δ 12.55 (s, 1H), 11.54 (s, 1H), 7.63–7.54 (m, 3H), 7.23 (dd, J = 8.4, 1.7 Hz, 1H), 3.38 (s, 2H). ^{13}C NMR (126 MHz, DMSO- d_6) δ 171.1, 163.0, 137.1, 132.0, 127.8, 122.6, 120.3, 114.6, 114.5, 103.0, 38.7. ESI-MS (m/z): 284.1 [$\text{M} - \text{H}$] $^-$.

4.2.8. 2-((7-Bromo-1H-indol-3-yl)thio)acetic acid **5f**

^1H NMR (500 MHz, DMSO- d_6) δ 12.48 (s, 1H), 11.69 (s, 1H), 7.65 (d, J = 7.9 Hz, 1H), 7.59 (d, J = 2.7 Hz, 1H), 7.39 (d, J = 7.5 Hz, 1H), 7.06 (t, J = 7.7 Hz, 1H). ^{13}C NMR (126 MHz, DMSO- d_6) δ 171.6, 135.0, 132.5, 131.0, 124.9, 121.6, 118.6, 105.1, 104.6, 39.1. ESI-MS (m/z): 284.2 [$\text{M} - \text{H}$] $^-$.

4.2.9. General procedure for the synthesis of **6a1-6**, **6b1-7**, **6c1-8**, **6d1-5**, and **6c9**

To a solution of compound **5** in dichloromethane (0.2 mmol/mL) was added DIEA (2.4 eq.), HATU (2.2 eq.) and substituted benzyl amine (1.1 eq.). The solution was stirred for 1 h at 25 °C and diluted with dichloromethane and washed with 30 mL of saturated sodium bicarbonate, sodium bicarbonate, 0.5 N hydrochloric acid and saturated sodium chloride solution in sequence. After purification on a silica column (PE/EA = 10:1–5:1) the target product was afforded.

4.2.10. N-benzyl-2-((1-methyl-1H-indol-3-yl)thio)acetamide **6a1**

Purity: 95.7%.

^1H NMR (400 MHz, DMSO- d_6) δ 8.34 (t, J = 5.9 Hz, 1H), 7.62 (dt, J = 7.8, 1.0 Hz, 1H), 7.51–7.46 (m, 1H), 7.45 (s, 1H), 7.31–7.17 (m, 4H), 7.16–7.06 (m, 3H), 4.21 (d, J = 5.9 Hz, 2H), 3.75 (s, 3H), 2.53–2.47 (m, 2H). ^{13}C NMR (101 MHz, DMSO- d_6) δ 169.1, 139.6, 137.3, 135.2, 128.6, 127.7, 127.2, 122.3, 120.2, 119.3, 110.7, 102.2, 42.8, 39.5, 33.1. HRMS (ESI) m/z calcd. for $\text{C}_{18}\text{H}_{18}\text{N}_2\text{OSNa}$ ($[\text{M} + \text{Na}]^+$): 333.1032, found 333.1045.

4.2.11. N,N-dibenzyl-2-((1-methyl-1H-indol-3-yl)thio)acetamide **6a2**

Purity: 96.6%.

^1H NMR (400 MHz, DMSO- d_6) δ 7.48 (dt, J = 8.2, 0.9 Hz, 1H), 7.45 (s, 1H), 7.37–7.25 (m, 6H), 7.25–7.21 (m, 1H), 7.19 (dt, J = 8.0, 1.2 Hz, 2H), 7.14–7.05 (m, 3H), 4.45 (s, 2H), 4.42 (s, 2H), 3.76 (s, 3H), 3.67 (s, 2H). ^{13}C NMR (101 MHz, DMSO- d_6) δ 169.5, 137.8, 137.3, 135.3, 129.1, 128.9, 128.2, 127.8, 127.6, 127.0, 122.4, 120.3, 119.0, 110.8, 50.7, 48.6, 38.8, 33.1. HRMS (ESI) m/z calcd. for $\text{C}_{25}\text{H}_{24}\text{N}_2\text{OSNa}$ ($[\text{M} + \text{Na}]^+$): 423.1501, found 423.1501.

4.2.12. 2-((1-Methyl-1H-indol-3-yl)thio)-N-(4-(trifluoromethyl)benzyl)acetamide **6a3**

Purity: 99.6%.

^1H NMR (400 MHz, DMSO- d_6) δ 8.49 (t, J = 6.0 Hz, 1H), 7.66–7.58 (m, 3H), 7.48 (s, 2H), 7.36–7.28 (m, 2H), 7.22 (ddd, J = 8.2, 7.0, 1.2 Hz, 1H), 7.12 (ddd, J = 8.0, 7.0, 1.0 Hz, 1H), 4.30 (d, J = 5.9 Hz, 2H), 3.75 (s, 3H), 3.36 (s, 2H). ^{13}C NMR (101 MHz, DMSO- d_6) δ 169.3, 144.6, 137.3, 135.2, 129.7, 128.3, 125.5, 122.3, 120.2, 119.2, 110.7, 102.1, 42.4, 40.5, 33.0. HRMS (ESI) m/z calcd. for $\text{C}_{19}\text{H}_{17}\text{F}_3\text{N}_2\text{OSNa}$ ($[\text{M} + \text{Na}]^+$): 401.0906, found 401.0894.

4.2.13. N-(4-(2-(dimethylamino)ethoxy)benzyl)-2-((1-methyl-1H-indol-3-yl)thio)acetamide **6a4**

Purity: 96.0%.

^1H NMR (500 MHz, DMSO- d_6) δ 8.27 (t, J = 5.9 Hz, 1H), 7.62 (d, J = 7.9 Hz, 1H), 7.50–7.41 (m, 2H), 7.25–7.18 (m, 1H), 7.16–7.08 (m, 1H), 7.04 (d, J = 8.5 Hz, 2H), 6.84 (d, J = 8.6 Hz, 2H), 4.14 (d, J = 5.8 Hz, 2H), 4.04 (t, J = 5.7 Hz, 2H), 3.75 (s, 3H), 3.18 (s, 2H), 2.73 (t, J = 5.7 Hz, 2H), 2.30 (s, 6H). ^{13}C NMR (126 MHz, DMSO- d_6) δ 169.0, 157.8, 137.3, 135.2, 131.8, 129.8, 129.2, 122.3, 120.3, 119.3, 114.7, 110.7, 102.3, 65.8, 57.9, 45.7, 40.7, 33.1. HRMS (ESI) m/z calcd. for $\text{C}_{22}\text{H}_{27}\text{N}_3\text{O}_2\text{SNa}$ ($[\text{M} + \text{Na}]^+$): 420.1716, found 420.1748.

4.2.14. N-(2-methoxybenzyl)-2-((1-methyl-1H-indol-3-yl)thio)acetamide **6a5**

Purity: 97.9%.

^1H NMR (400 MHz, DMSO- d_6) δ 8.21–8.13 (m, 1H), 7.63 (ddd, J = 8.0, 2.2, 1.2 Hz, 1H), 7.51–7.42 (m, 2H), 7.22 (td, J = 7.8, 1.2 Hz, 2H), 7.12 (tt, J = 7.1, 1.1 Hz, 1H), 6.99–6.89 (m, 2H), 6.86–6.77 (m, 1H), 4.22–4.15 (m, 2H), 3.77 (s, 3H), 3.75 (s, 3H), 3.39–3.35 (m, 2H). ^{13}C NMR (101 MHz, DMSO- d_6) δ 169.1, 157.0, 137.3, 135.1, 128.4, 128.0, 126.9, 122.3, 120.5, 120.2, 119.2, 110.8, 110.7, 102.2, 55.7, 40.5, 37.9, 33.1. HRMS (ESI) m/z calcd. for $\text{C}_{19}\text{H}_{20}\text{N}_2\text{O}_2\text{SNa}$ ($[\text{M} + \text{Na}]^+$): 363.1137, found 363.1130.

4.2.15. N-(3,4-dichlorobenzyl)-2-((1-methyl-1H-indol-3-yl)thio)acetamide **6a6**

Purity: 99.5%.

^1H NMR (400 MHz, DMSO- d_6) δ 8.46 (t, J = 6.0 Hz, 1H), 7.64–7.57 (m, 1H), 7.53 (d, J = 8.3 Hz, 1H), 7.48 (dt, J = 8.1, 0.9 Hz, 1H), 7.46 (s, 1H), 7.41 (d, J = 2.0 Hz, 1H), 7.22 (ddd, J = 8.2, 7.0, 1.2 Hz, 1H), 7.11 (ddd, J = 8.2, 5.2, 1.5 Hz, 2H), 4.21 (d, J = 5.9 Hz, 2H), 3.76 (s, 3H), 3.36–3.34 (m, 2H). ^{13}C NMR (101 MHz, DMSO- d_6) δ 169.4, 141.0, 137.3, 135.1, 131.2, 130.8, 129.7, 129.1, 128.1, 122.3, 120.2, 119.2, 110.8, 102.1, 41.8, 40.5, 33.1. HRMS (ESI) m/z calcd. for $\text{C}_{18}\text{H}_{16}\text{Cl}_2\text{N}_2\text{OS}$ ($[\text{M} + \text{Na}]^+$): 401.0252, found 401.0253.

4.2.16. N-benzyl-2-((1H-indol-3-yl)thio)acetamide **6b1**

Purity: 95.2%.

^1H NMR (400 MHz, DMSO- d_6) δ 11.39 (s, 1H), 8.36 (t, J = 5.9 Hz, 1H), 7.62 (dt, J = 7.7, 1.0 Hz, 1H), 7.47 (d, J = 2.6 Hz, 1H), 7.45–7.40 (m, 1H), 7.30–7.19 (m, 3H), 7.15 (ddd, J = 8.2, 7.0, 1.3 Hz, 1H), 7.13–7.06 (m, 3H), 4.22 (d, J = 5.9 Hz, 2H), 3.36 (s, 2H). ^{13}C NMR (101 MHz, DMSO- d_6) δ 169.1, 139.6, 136.7, 131.2, 129.3, 128.6, 127.6,

127.1, 122.2, 120.0, 119.0, 112.4, 103.2, 42.8, 40.5. HRMS (ESI) m/z calcd. for $C_{17}H_{16}N_2OSNa$ ($[M + Na]^+$): 319.0875, found 319.0872.

4.2.17. *N,N*-dibenzyl-2-((1*H*-indol-3-yl)thio)acetamide **6b2**

Purity: 92.7%.

1H NMR (400 MHz, DMSO- d_6) δ 11.41 (s, 1H), 7.58–7.51 (m, 1H), 7.47 (d, $J = 2.7$ Hz, 1H), 7.45–7.41 (m, 1H), 7.37–7.24 (m, 6H), 7.21–7.11 (m, 3H), 7.11–7.02 (m, 3H), 4.44 (d, $J = 6.9$ Hz, 4H), 3.67 (s, 2H). ^{13}C NMR (101 MHz, DMSO- d_6) δ 169.6, 137.8, 137.3, 136.8, 131.4, 129.2, 129.1, 128.9, 128.1, 127.8, 127.5, 127.0, 122.3, 120.2, 118.8, 112.5, 102.5, 50.8, 48.5, 38.7. HRMS (ESI) m/z calcd. for $C_{24}H_{22}N_2OSNa$ ($[M + Na]^+$): 409.1345, found 409.1336.

4.2.18. 2-((1*H*-indol-3-yl)thio)-*N*-(4-(trifluoromethyl)benzyl)acetamide **6b3**

Purity: 95.5%.

1H NMR (400 MHz, DMSO- d_6) δ 11.43 (s, 1H), 8.49 (t, $J = 6.0$ Hz, 1H), 7.67–7.57 (m, 3H), 7.52 (d, $J = 2.6$ Hz, 1H), 7.44 (dt, $J = 8.1$, 1.0 Hz, 1H), 7.32–7.24 (m, 2H), 7.16 (ddd, $J = 8.2$, 7.1, 1.3 Hz, 1H), 7.08 (ddd, $J = 8.0$, 7.0, 1.1 Hz, 1H), 4.31 (d, $J = 5.9$ Hz, 2H), 3.39 (s, 2H). ^{13}C NMR (101 MHz, DMSO) δ 169.4, 144.6, 136.8, 131.3, 129.3, 128.1, 125.5, 125.5, 125.4, 125.4, 122.2, 120.1, 119.0, 112.5, 103.0, 42.4, 38.7. HRMS (ESI) m/z calcd. for $C_{18}H_{15}F_3N_2OSNa$ ($[M + Na]^+$): 387.0749, found 387.0743.

4.2.19. *N*-(4-(2-(dimethylamino)ethoxy)benzyl)-2-((1*H*-indol-3-yl)thio)acetamide **6b4**

Purity: 97.9%

1H NMR (400 MHz, DMSO- d_6) δ 8.28 (t, $J = 5.9$ Hz, 1H), 7.61 (ddt, $J = 7.7$, 1.4, 0.7 Hz, 1H), 7.47 (d, $J = 2.6$ Hz, 1H), 7.43 (dt, $J = 8.1$, 0.9 Hz, 1H), 7.15 (ddd, $J = 8.2$, 7.0, 1.3 Hz, 1H), 7.08 (ddd, $J = 8.0$, 7.0, 1.1 Hz, 1H), 7.04–6.98 (m, 2H), 6.86–6.79 (m, 2H), 4.14 (d, $J = 5.8$ Hz, 2H), 4.02 (t, $J = 5.8$ Hz, 2H), 2.63 (t, $J = 5.8$ Hz, 2H), 2.23 (s, 6H). ^{13}C NMR (101 MHz, DMSO- d_6) δ 169.0, 157.8, 136.7, 131.6, 131.2, 129.3, 128.9, 122.2, 120.0, 119.0, 114.6, 112.4, 103.2, 66.1, 58.1, 45.9, 42.2, 40.5. HRMS (ESI) m/z calcd. for $C_{21}H_{26}N_3O_2S$ ($[M + H]^+$): 384.1740, found 384.1760.

4.2.20. 2-((1*H*-indol-3-yl)thio)-*N*-benzyl-*N*-methylacetamide **6b5**

Purity: 99.7%.

1H NMR (500 MHz, DMSO- d_6) δ 11.41 (s, 1H), 7.59 (major) + 7.55 (minor) (d, $J = 7.9$ Hz, 1H), 7.51 (dt, $J = 15.7$, 2.6 Hz, 1H), 7.43 (dd, $J = 8.2$, 2.7 Hz, 1H), 7.36–7.29 (m, 2H), 7.26 (dt, $J = 9.3$, 4.7 Hz, 1H), 7.20–7.04 (m, 4H), 4.47 (minor) + 4.45 (major) (bs, 2H), 3.66 (major) + 3.62 (minor) (bs, 2H), 2.86 (major) + 2.73 (minor) (s, 3H). ^{13}C NMR (126 MHz, DMSO- d_6) δ 169.2, 138.0, 136.8, 131.5, 129.4, 129.1, 128.9, 128.0, 127.8, 127.5, 127.1, 122.3, 120.2, 118.9, 112.6, 102.6, 53.3, 50.6, 38.9, 38.8, 35.7, 33.9. Rotamers formed because of tertiary amides in the structure which was similar to that reported in literature [39,40]. HRMS (ESI) m/z calcd. for $C_{18}H_{18}N_2OSNa$ ($[M + Na]^+$): 333.1032, found 333.1031.

4.2.21. 2-((1*H*-indol-3-yl)thio)-*N*-(2-methoxybenzyl)-*N*-methylacetamide **6b6**

Purity: 99.6%.

1H NMR (500 MHz, DMSO- d_6) δ 11.40 (s, 1H), 7.64 (major) + 7.54 (minor) (d, $J = 7.9$ Hz, 1H), 7.50 (dd, $J = 7.7$, 2.5 Hz, 1H), 7.42 (dd, $J = 8.1$, 4.8 Hz, 1H), 7.25 (q, $J = 8.3$, 7.7 Hz, 1H), 7.19–7.12 (m, 1H), 7.09 (dt, $J = 17.2$, 7.5 Hz, 1H), 7.03–6.95 (m, 2H), 6.94–6.87 (m, 1H), 4.40 (major) + 4.37 (minor) (s, 2H), 3.78 (major) + 3.72 (minor) (s, 3H), 3.67 (major) + 3.60 (minor) (s, 2H), 2.91 (major) + 2.73 (minor) (s, 3H). ^{13}C NMR (126 MHz, DMSO- d_6) δ 169.2, 157.4, 157.3, 136.8, 131.4, 129.4, 129.2, 128.6, 127.9, 127.7, 125.4, 124.9, 122.3, 120.9, 120.7, 120.2, 120.1, 118.9, 118.8, 112.5, 111.3, 111.1, 102.8, 102.7, 55.8, 55.7, 46.0, 39.0, 38.9, 36.3, 33.8. Rotamers formed because of tertiary

amides in the structure which was similar to that reported in literature [39,40]. HRMS (ESI) m/z calcd. for $C_{19}H_{20}N_2O_2SNa$ ($[M + Na]^+$): 363.1137, found 363.1145.

4.2.22. (*R*)-2-((1*H*-indol-3-yl)thio)-*N*-(1-phenylethyl)acetamide **6b7**

1H NMR (400 MHz, DMSO- d_6) δ 11.37 (s, 1H), 8.22 (d, $J = 8.0$ Hz, 1H), 7.60 (ddd, $J = 7.8$, 1.4, 0.7 Hz, 1H), 7.45–7.37 (m, 2H), 7.32–7.23 (m, 2H), 7.25–7.15 (m, 3H), 7.14 (ddd, $J = 8.2$, 7.0, 1.3 Hz, 1H), 7.07 (ddd, $J = 7.9$, 7.0, 1.1 Hz, 1H), 4.83 (p, $J = 7.2$ Hz, 1H), 3.33 (s, 2H), 1.22 (d, $J = 7.1$ Hz, 3H). ^{13}C NMR (101 MHz, DMSO- d_6) δ 168.2, 144.8, 136.7, 131.2, 129.4, 128.6, 127.0, 126.4, 122.2, 120.0, 119.1, 112.4, 103.2, 48.4, 38.7, 22.6. HRMS (ESI) m/z calcd. for $C_{18}H_{18}N_2OSNa$ ($[M + Na]^+$): 333.1032, found 333.1041.

4.2.23. 2-((4-Bromo-1*H*-indol-3-yl)thio)-*N*-(2-methoxybenzyl)acetamide **6c1**

Purity: 95.2%.

1H NMR (400 MHz, DMSO- d_6) δ 11.74–11.68 (bs, 1H), 8.22 (t, $J = 5.9$ Hz, 1H), 7.54–7.42 (m, 2H), 7.27 (dd, $J = 7.6$, 0.8 Hz, 1H), 7.22 (ddd, $J = 8.2$, 7.3, 1.8 Hz, 1H), 7.05 (t, $J = 7.8$ Hz, 1H), 6.95 (ddd, $J = 7.8$, 4.9, 1.4 Hz, 2H), 6.84 (td, $J = 7.4$, 1.1 Hz, 1H), 4.20 (d, $J = 5.9$ Hz, 2H), 3.78 (s, 3H), 3.48 (s, 2H). ^{13}C NMR (101 MHz, DMSO- d_6) δ 168.7, 156.9, 138.3, 133.2, 128.4, 127.8, 127.0, 125.8, 124.6, 123.4, 120.5, 113.4, 112.4, 110.8, 103.8, 55.7, 42.1, 37.8. HRMS (ESI) m/z calcd. for $C_{18}H_{17}BrN_2O_2SNa$ ($[M + Na]^+$): 427.0086, found 427.0091.

4.2.24. 2-((4-Bromo-1*H*-indol-3-yl)thio)-*N*-(3,4-dichlorobenzyl)acetamide **6c2**

Purity: 95.7%.

1H NMR (400 MHz, DMSO- d_6) δ 11.75 (s, 1H), 8.51 (t, $J = 6.0$ Hz, 1H), 7.57–7.50 (m, 2H), 7.46 (dd, $J = 8.2$, 0.9 Hz, 1H), 7.43 (d, $J = 2.0$ Hz, 1H), 7.27 (dd, $J = 7.6$, 0.8 Hz, 1H), 7.10 (dd, $J = 8.3$, 2.1 Hz, 1H), 7.05 (t, $J = 7.8$ Hz, 1H), 4.24 (d, $J = 6.0$ Hz, 2H), 3.46 (s, 2H). ^{13}C NMR (101 MHz, DMSO- d_6) δ 169.0, 141.2, 138.3, 133.3, 131.3, 130.8, 129.6, 129.4, 127.8, 125.8, 124.6, 123.4, 113.4, 112.4, 103.7, 42.1, 41.6. HRMS (ESI) m/z calcd. for $C_{17}H_{13}BrCl_2N_2OSNa$ ($[M + Na]^+$): 464.9201, found 464.9228.

4.2.25. 2-((5-Bromo-1*H*-indol-3-yl)thio)-*N*-(2-methoxybenzyl)acetamide **6c3**

Purity: 94.9%.

1H NMR (400 MHz, DMSO- d_6) δ 11.64–11.58 (m, 1H), 8.19 (t, $J = 5.8$ Hz, 1H), 7.81–7.75 (m, 1H), 7.54 (d, $J = 2.6$ Hz, 1H), 7.41 (dd, $J = 8.6$, 0.6 Hz, 1H), 7.27 (dd, $J = 8.6$, 2.0 Hz, 1H), 7.21 (ddd, $J = 8.2$, 7.3, 1.8 Hz, 1H), 6.95 (dd, $J = 8.2$, 1.0 Hz, 1H), 6.90 (dd, $J = 7.5$, 1.8 Hz, 1H), 6.83 (td, $J = 7.4$, 1.1 Hz, 1H), 4.18 (d, $J = 5.8$ Hz, 2H), 3.78 (s, 3H), 3.38 (s, 2H). ^{13}C NMR (101 MHz, DMSO- d_6) δ 169.1, 157.0, 135.5, 132.9, 131.3, 128.4, 127.9, 126.8, 124.8, 121.4, 120.5, 114.5, 113.0, 110.8, 103.0, 55.7, 38.7, 37.9. HRMS (ESI) m/z calcd. for $C_{18}H_{17}BrN_2O_2SNa$ ($[M + Na]^+$): 427.0086, found 427.0090.

4.2.26. 2-((5-Bromo-1*H*-indol-3-yl)thio)-*N*-(3,4-dichlorobenzyl)acetamide **6c4**

Purity: 98.5%.

1H NMR (400 MHz, DMSO- d_6) δ 11.62 (d, $J = 2.7$ Hz, 1H), 8.47 (t, $J = 5.9$ Hz, 1H), 7.78–7.72 (m, 1H), 7.56 (d, $J = 2.6$ Hz, 1H), 7.51 (d, $J = 8.3$ Hz, 1H), 7.40 (dd, $J = 8.6$, 0.6 Hz, 1H), 7.37 (d, $J = 2.1$ Hz, 1H), 7.26 (dd, $J = 8.6$, 1.9 Hz, 1H), 7.04 (dd, $J = 8.3$, 2.1 Hz, 1H), 4.21 (d, $J = 5.9$ Hz, 2H), 3.36 (s, 2H). ^{13}C NMR (101 MHz, DMSO- d_6) δ 169.4, 140.9, 135.5, 133.0, 131.3, 131.2, 130.8, 129.7, 129.5, 127.8, 124.8, 121.3, 114.6, 113.0, 102.8, 41.7, 38.7. HRMS (ESI) m/z calcd. for $C_{17}H_{13}BrCl_2N_2OSNa$ ($[M + Na]^+$): 464.9201, found 464.9261.

4.2.27. 2-((6-Bromo-1H-indol-3-yl)thio)-N-(2-methoxybenzyl)acetamide **6c5**

Purity: 95.5%.

^1H NMR (400 MHz, DMSO- d_6) δ 11.52 (s, 1H), 8.17 (t, J = 5.9 Hz, 1H), 7.61 (dd, J = 1.8, 0.5 Hz, 1H), 7.58–7.53 (m, 1H), 7.50 (d, J = 2.6 Hz, 1H), 7.27–7.16 (m, 2H), 6.95 (dd, J = 8.2, 1.0 Hz, 1H), 6.89 (dd, J = 7.5, 1.9 Hz, 1H), 6.82 (td, J = 7.4, 1.1 Hz, 1H), 4.17 (d, J = 5.8 Hz, 2H), 3.78 (s, 3H), 3.38 (s, 2H). ^{13}C NMR (101 MHz, DMSO- d_6) δ 169.1, 157.0, 137.6, 132.2, 128.4, 128.4, 128.0, 126.8, 123.0, 120.9, 120.5, 115.0, 114.9, 110.8, 103.8, 55.7, 38.7, 37.9. HRMS (ESI) m/z calcd. for $\text{C}_{18}\text{H}_{17}\text{BrN}_2\text{O}_2\text{SNa}$ ($[\text{M} + \text{Na}]^+$): 427.0086, found 427.0107.

4.2.28. 2-((6-Bromo-1H-indol-3-yl)thio)-N-(3,4-dichlorobenzyl)acetamide **6c6**

Purity: 97.8%.

^1H NMR (400 MHz, DMSO- d_6) δ 11.53 (d, J = 2.5 Hz, 1H), 8.45 (t, J = 6.0 Hz, 1H), 7.61 (dd, J = 1.8, 0.5 Hz, 1H), 7.57–7.48 (m, 3H), 7.38 (d, J = 2.0 Hz, 1H), 7.19 (dd, J = 8.4, 1.8 Hz, 1H), 7.04 (dd, J = 8.3, 2.0 Hz, 1H), 4.20 (d, J = 5.9 Hz, 2H), 3.36 (s, 2H). ^{13}C NMR (101 MHz, DMSO- d_6) δ 169.4, 140.9, 137.6, 132.3, 131.2, 130.7, 129.7, 129.5, 128.4, 127.9, 123.0, 120.8, 115.1, 115.0, 103.6, 41.7, 38.7. HRMS (ESI) m/z calcd. for $\text{C}_{17}\text{H}_{13}\text{BrCl}_2\text{N}_2\text{OSNa}$ ($[\text{M} + \text{Na}]^+$): 464.9201, found 464.9234.

4.2.29. 2-((7-Bromo-1H-indol-3-yl)thio)-N-(2-methoxybenzyl)acetamide **6c7**

Purity: 99.3%.

^1H NMR (400 MHz, DMSO- d_6) δ 11.69–11.63 (m, 1H), 8.17 (t, J = 5.9 Hz, 1H), 7.66–7.59 (m, 1H), 7.53 (dd, J = 2.8, 1.0 Hz, 1H), 7.38 (dd, J = 7.6, 0.8 Hz, 1H), 7.21 (ddd, J = 8.2, 7.1, 2.0 Hz, 1H), 7.04 (t, J = 7.7 Hz, 1H), 6.94 (dd, J = 8.3, 1.0 Hz, 1H), 6.90–6.77 (m, 2H), 4.16 (d, J = 5.7 Hz, 2H), 3.40 (d, J = 1.1 Hz, 2H). ^{13}C NMR (101 MHz, DMSO- d_6) δ 169.0, 157.0, 135.0, 132.3, 131.1, 128.4, 127.9, 126.8, 124.8, 121.5, 120.5, 118.7, 110.8, 105.0, 104.9, 55.7, 40.2, 37.8. HRMS (ESI) m/z calcd. for $\text{C}_{18}\text{H}_{17}\text{BrN}_2\text{O}_2\text{SNa}$ ($[\text{M} + \text{Na}]^+$): 427.0086, found 427.0099.

4.2.30. 2-((7-Bromo-1H-indol-3-yl)thio)-N-(3,4-dichlorobenzyl)acetamide **6c8**

Purity: 99.2%.

^1H NMR (400 MHz, DMSO- d_6) δ 11.69–11.64 (m, 1H), 8.46 (t, J = 6.0 Hz, 1H), 7.61 (dt, J = 7.9, 0.8 Hz, 1H), 7.54 (d, J = 2.7 Hz, 1H), 7.49 (d, J = 8.3 Hz, 1H), 7.41–7.34 (m, 2H), 7.07–6.96 (m, 2H), 4.19 (d, J = 6.0 Hz, 2H), 3.38 (s, 2H). ^{13}C NMR (101 MHz, DMSO- d_6) δ 169.3, 141.0, 135.0, 132.4, 131.2, 131.0, 130.7, 129.6, 129.5, 127.8, 124.9, 121.5, 118.6, 105.1, 104.7, 41.7. HRMS (ESI) m/z calcd. for $\text{C}_{17}\text{H}_{13}\text{BrCl}_2\text{N}_2\text{OSNa}$ ($[\text{M} + \text{Na}]^+$): 464.9201, found 464.9249.

4.2.31. N-benzyl-2-((4-bromo-1H-indol-3-yl)thio)-N-methylacetamide **6d1**

Purity: 96.8%.

^1H NMR (400 MHz, DMSO- d_6) δ 11.73 (s, 1H), 7.59 (minor) + 7.53 (major) (d, J = 2.7 Hz, 1H), 7.46 (major) + 7.44 (minor) (dd, J = 8.1, 0.9 Hz, 1H), 7.33 (m, 2H), 7.29–7.22 (m, 2H), 7.20–7.14 (m, 2H), 7.08–7.00 (m, 1H), 4.56 (minor) + 4.46 (major) (s, 2H), 3.79 (major) + 3.72 (minor) (s, 2H), 2.92 (major) + 2.76 (minor) (s, 3H). ^{13}C NMR (101 MHz, DMSO- d_6) δ 168.7, 168.6, 138.3, 138.3, 138.0, 137.6, 133.6, 133.6, 129.1, 128.9, 127.9, 127.7, 127.5, 127.1, 126.1, 124.6, 124.6, 123.4, 113.3, 112.4, 112.4, 103.4, 103.2, 53.3, 50.5, 41.2, 40.8, 38.7, 35.7, 33.8. Rotamers formed because of tertiary amides in the structure which was similar to that reported in literature [39,40]. HRMS (ESI) m/z calcd. for $\text{C}_{18}\text{H}_{17}\text{BrN}_2\text{OSNa}$ ($[\text{M} + \text{Na}]^+$): 411.0137, found 411.0181.

4.2.32. N,N-dibenzyl-2-((4-bromo-1H-indol-3-yl)thio)acetamide **6d2**

Purity: 97.7%.

^1H NMR (400 MHz, DMSO- d_6) δ 11.75 (d, J = 2.8 Hz, 1H), 7.54 (d, J = 2.7 Hz, 1H), 7.45 (dd, J = 8.1, 0.9 Hz, 1H), 7.38–7.28 (m, 5H), 7.28–7.22 (m, 2H), 7.15 (tt, J = 6.3, 1.4 Hz, 4H), 7.05 (t, J = 7.8 Hz, 1H), 4.47 (d, J = 12.3 Hz, 4H), 3.77 (s, 2H). ^{13}C NMR (101 MHz, DMSO- d_6) δ 169.1, 138.3, 137.8, 137.3, 133.8, 129.2, 128.9, 128.0, 127.8, 127.5, 127.0, 124.7, 123.5, 112.5, 103.0, 50.7, 48.5, 41.0. HRMS (ESI) m/z calcd. for $\text{C}_{24}\text{H}_{21}\text{BrN}_2\text{OSNa}$ ($[\text{M} + \text{Na}]^+$): 487.0450, found 487.0474.

4.2.33. N-benzyl-2-((7-bromo-1H-indol-3-yl)thio)-N-methylacetamide **6d3**

Purity: 99.5%.

^1H NMR (400 MHz, DMSO- d_6) δ 11.68 (s, 1H), 7.66–7.52 (m, 2H), 7.38 (td, J = 7.1, 6.6, 0.9 Hz, 1H), 7.35–7.29 (m, 2H), 7.29–7.22 (m, 1H), 7.19–7.09 (m, 2H), 7.06 (major) + 7.03 (minor) (t, J = 7.8 Hz, 1H), 4.51 (minor) + 4.44 (major) (s, 2H), 3.70 (major) + 3.66 (minor) (s, 2H), 2.88 major + 2.72 (minor) (s, 3H). ^{13}C NMR (101 MHz, DMSO- d_6) δ 169.0, 168.9, 137.9, 137.6, 135.0, 132.5, 131.1, 129.1, 128.9, 127.9, 127.7, 127.5, 127.1, 124.9, 124.9, 121.6, 121.6, 118.6, 118.5, 105.1, 104.5, 104.3, 53.3, 50.5, 38.8, 38.7, 38.7, 35.7, 33.9. Rotamers formed because of tertiary amides in the structure which was similar to that reported in literature [39,40]. HRMS (ESI) m/z calcd. for $\text{C}_{18}\text{H}_{17}\text{BrN}_2\text{OSNa}$ ($[\text{M} + \text{Na}]^+$): 411.0137, found 411.0181.

4.2.34. N,N-dibenzyl-2-((7-bromo-1H-indol-3-yl)thio)acetamide **6d4**

Purity: 96.5%.

^1H NMR (400 MHz, DMSO- d_6) δ 11.68 (d, J = 2.8 Hz, 1H), 7.59–7.51 (m, 2H), 7.38 (dd, J = 7.6, 0.9 Hz, 1H), 7.34–7.22 (m, 6H), 7.15–7.11 (m, 2H), 7.10–7.06 (m, 2H), 7.01 (t, J = 7.7 Hz, 1H), 4.44 (d, J = 8.3 Hz, 4H), 3.71 (s, 2H). ^{13}C NMR (101 MHz, DMSO- d_6) δ 169.4, 137.7, 137.3, 135.0, 132.5, 131.0, 129.1 \times 2, 128.9 \times 2, 128.0 \times 2, 127.8, 127.5, 127.0 \times 2, 124.9, 121.6, 118.5, 105.1, 104.3, 50.8, 48.5, 38.6. HRMS (ESI) m/z calcd. for $\text{C}_{24}\text{H}_{21}\text{BrN}_2\text{OSNa}$ ($[\text{M} + \text{Na}]^+$): 487.0450, found 487.0472.

4.2.35. N-(2-ethoxybenzyl)-2-((4-bromo-1H-indol-3-yl)thio)-N-methoxyacetamide **6d5**

Purity: 96.2%.

^1H NMR (400 MHz, DMSO- d_6) δ 11.73 (s, 1H), 7.54 (s, 1H), 7.45 (dd, J = 8.1, 0.8 Hz, 1H), 7.31–7.19 (m, 2H), 7.12–6.99 (m, 2H), 6.96 (dd, J = 8.3, 1.0 Hz, 1H), 6.87 (td, J = 7.5, 1.1 Hz, 1H), 4.02 (q, J = 6.9 Hz, 2H), 3.75 (s, 2H), 3.57 (s, 3H), 1.32 (t, J = 6.8 Hz, 3H). ^{13}C NMR (101 MHz, DMSO- d_6) δ 169.5, 156.7, 138.3, 133.8, 129.0, 128.8, 125.9, 124.7, 124.5, 123.4, 120.5, 113.3, 112.5, 112.0, 103.4, 63.7, 62.0, 42.8, 38.7, 15.1. HRMS (ESI) m/z calcd. for $\text{C}_{19}\text{H}_{19}\text{BrN}_2\text{O}_3\text{SNa}$ ($[\text{M} + \text{Na}]^+$): 471.0348, found 471.0437.

4.2.36. Synthesis of compound N-(2-methoxybenzyl)-2-((7-phenyl-1H-indol-3-yl)thio)acetamide **6c9**

Purity: 99.7%.

6c8 (442 mg, 1 mmol), phenylboronic acid (146 mg, 1.2 mmol), $\text{Pd}_2(\text{dba})_3$ (18 mg, 0.02 mmol), SPhps (16 mg, 0.04 mmol) and Cs_2CO_3 (651 mg, 2 mmol) were dissolved in 1,4-dioxane (2 mL) under Ar. The mixture was stirred for 3 h at 125 °C in a CEM microwave reactor. After purification on a silica column the target product was afforded. (306 mg, 76.2%).

^1H NMR (400 MHz, DMSO- d_6) δ 11.29 (d, J = 2.8 Hz, 1H), 8.21 (t, J = 5.9 Hz, 1H), 7.68–7.59 (m, 3H), 7.57–7.49 (m, 2H), 7.48–7.41 (m, 2H), 7.25–7.15 (m, 3H), 6.96 (ddd, J = 11.1, 7.8, 1.4 Hz, 2H), 6.82 (td, J = 7.4, 1.1 Hz, 1H), 4.19 (d, J = 5.8 Hz, 2H), 3.42 (s, 2H), 2.50 (p, J = 1.8 Hz, 2H). ^{13}C NMR (101 MHz, DMSO- d_6) δ 169.2, 157.0, 138.7, 133.9, 131.9, 130.2, 129.4, 128.7, 128.4, 128.0, 127.8, 126.9, 126.4,

122.5, 120.7, 120.5, 118.5, 110.8, 103.9, 55.7, 38.7, 37.9. HRMS (ESI) m/z calcd. for $C_{24}H_{22}N_2O_2SNa$ ($[M + Na]^+$): 425.1294, found 425.1294.

4.3. Cells, viruses, and transfection

Traditionally, HEK293T, HCT-8 and LLC-MK2 cells were grown in Dulbecco's modified Eagle's medium (DMEM; Gibco, Thermo Fisher Scientific, Waltham, MA, USA) supplemented with 10% (v/v) fetal bovine serum (FBS; Gibco). Cells were cultured at 37 °C in the incubator supplied with 5% of CO₂. Plasmid were transfected using the VigoFect transfection reagent (Beijing Vigorous, Beijing, China) according to the manufacturer's instructions. HCT-8 cells were infected with HCoV-OC43 (VR-1558) at a multiplicity of infection (MOI) of 0.1 and LLC-MK2 cells were infected with HCoV-NL63 strain Amsterdam I at an MOI of 0.01.

4.4. Plasmids, compounds and reagents

The codon-optimized pCOVID19-nsp12, pCOVID19-nsp7, pCOVID19-nsp8, pCOVID19-nsp10 and pCOVID19-nsp14 was encoding a flag-tagged nsp12, nsp7, nsp8, nsp10 and nsp14 at its C-terminus, respectively. The plasmid pCoV-Gluc which is the transcription of Gaussia-luciferase (Gluc) as the reporter gene flanked by 5' and 3' untranslated regions (UTRs) of SARS-CoV-2 is initiated by the CMV (cytomegalovirus) promoter. Briefly, 5'UTR-Gluc-3'UTR was inserted into the BamHI and NotI sites of pRetroX-tight-Pur vector (kindly provided by Dr. Guo Fei). The primers are upper (5'-GGC GGA TCC ATT AAA GGT TTA TAC-3') and lower (5'-TTA GCG GCC GCG TCA TTC TCC TAA GAA-3'). The compounds were synthesized in our lab and Remdesivir (S8932) were obtained from Selleck chemicals (Houston, TX, USA) and prepared in DMSO.

4.5. Gluc activity assay and real-time RNA isolation and quantitative RT-PCR

The experiments were performed in accordance with the standard procedure we previously reported [38].

4.6. Cell toxicity assay

The cell viability was evaluated by cell countingkit-8 (CCK-8, Beyotime) assay. HEK293T cells were cultured in a 96-well plate and incubated with 1L of each tested compound ranging from 0.78 μM to 100 μM and incubated for 24 h. Then 10 μL of CCK-8 solution was added to each well and incubated for an additional 1 h at 37 °C. The optical density (OD) at 450 nm of each well was measured using the Enspire 2300 Multiplate reader (PekinElmer). Cells cultured in the medium with DMSO only were taken as the control. The half-maximal cytotoxic concentration (CC₅₀) for each compound was calculated by comparing the viability of compounds-treated cells with that of DMSO-treated cells.

4.7. Anti-coronavirus activity assay

The anti-coronavirus activity of the different strains was measured by MTS Cell Proliferation Colorimetric Assay kits (Promega, Madison, WI, USA). Briefly, HCT-8 cells were inoculated with HCoV-OC43 at a multiplicity of infection (MOI) of 0.1 and LLC-MK2 cells were inoculated with HCoV-NL63 at an MOI 0.01. After incubated in 2% FBS and each of test compounds for 120 h at 33 °C in 5% CO₂ incubator, 20 μL of MTS Cell Proliferation Colorimetric reagent was added into each well and incubated for another 3 h at 37 °C. The absorbance at 490 nm was measured using the Enspire 2300 Multiplate reader (PekinElmer).

4.8. Statistical analysis

Data are presented as the means ± SD from at least three independent experiments and statistical analyses were performed using a two-tailed Student's t-test. Differences between groups were considered statistically significant if $p < 0.01$ (**), $p < 0.001$ (***).

4.9. Molecular modeling studies

The cryo-electron microscopy structure of SARS-CoV-2 RdRp (PDB ID: 6M71) was prepared for docking using AutoDockTools (ADT, version: 1.5.6) by removing co-crystallized water molecules, adding polar hydrogens, and merging Gasteiger charges. The active site of SARS-CoV-2 RdRp was defined as a box of 26 Å × 26 Å × 26 Å, centered near the active sites ($x = 123.6$ Å, $y = 117.84$ Å, $z = 133.6$ Å). For each compound, we sampled the torsion angles of all rotatable bonds to generate multiple conformations. Each conformation was then assigned hydrogen appropriate for pH 7.4 and converted to PDBQT format input file using Open Babel (version 2.3.2). Molecular docking study was performed by using Auto Dock Vina software as previously described [41]. The final docked structure with the best binding energy (ΔG_{ADV}) was selected for each compound. The protein-ligand interactions were visually inspected by using PyMOL (version 2.3.4) and Free Maestro (version 11.8.012).

Declaration of competing interest

The authors declare that they have no known competing financial interests or personal relationships that could have appeared to influence the work reported in this paper.

Acknowledgments

The research was supported by the National Natural Science Foundation of China (grant number 81703366 ZGN), National Science & Technology Major Project "Key New Drug Creation and Manufacturing Program", China (Numbers: 2019ZX09201001-003 WYC, 2019ZX09721001-004-006) and the Fundamental Research Funds for the Central Universities (33320200046).

Appendix A. Supplementary data

Supplementary data to this article can be found online at <https://doi.org/10.1016/j.ejmech.2021.113622>.

References

- [1] World Health Organization, WHO coronavirus (COVID-19) dashboard. <https://covid19.who.int/>. (Accessed 14 May 2021).
- [2] J.H. Beigel, K.M. Tomashek, L.E. Dodd, A.K. Mehta, B.S. Zingman, A.C. Kalil, E. Hohmann, H.Y. Chu, A. Luetkemeyer, S. Kline, D. Lopez de Castilla, R.W. Finberg, K. Dierberg, V. Tapson, L. Hsieh, T.F. Patterson, R. Paredes, D.A. Sweeney, W.R. Short, G. Touloumi, D.C. Lye, N. Ohmagari, M.D. Oh, G.M. Ruiz-Palacios, T. Benfield, G. Fatkenheuer, M.G. Kortepeter, R.L. Atmar, C.B. Creech, J. Lundgren, A.G. Babiker, S. Pett, J.D. Neaton, T.H. Burgess, T. Bonnett, M. Green, M. Makowski, A. Osinusi, S. Nayak, H.C. Lane, A.-S.G. Members, Remdesivir for the treatment of covid-19 - final report, N. Engl. J. Med. 383 (2020) 1813–1826.
- [3] C.D. Spinner, R.L. Gottlieb, G.J. Criner, J.R. Arribas Lopez, A.M. Cattelan, A. Soriano Viladomiu, O. Ogbuagu, P. Malhotra, K.M. Mullane, A. Castagna, L.Y.A. Chai, M. Roestenberg, O.T.Y. Tsang, E. Bernasconi, P. Le Turnier, S.C. Chang, D. SenGupta, R.H. Hyland, A.O. Osinusi, H. Cao, C. Blair, H. Wang, A. Gaggar, D.M. Brainard, M.J. McPhail, S. Bhagani, M.Y. Ahn, A.J. Sanyal, G. Huhn, F.M. Marty, G.-U.- Investigators, Effect of remdesivir vs standard care on clinical status at 11 Days in patients with moderate COVID-19: a randomized clinical trial, J. Am. Med. Assoc. 324 (2020) 1048–1057.
- [4] Y. Wang, D. Zhang, G. Du, R. Du, J. Zhao, Y. Jin, S. Fu, L. Gao, Z. Cheng, Q. Lu, Y. Hu, G. Luo, K. Wang, Y. Lu, H. Li, S. Wang, S. Ruan, C. Yang, C. Mei, Y. Wang,

- D. Ding, F. Wu, X. Tang, X. Ye, Y. Ye, B. Liu, J. Yang, W. Yin, A. Wang, G. Fan, F. Zhou, Z. Liu, X. Gu, J. Xu, L. Shang, Y. Zhang, L. Cao, T. Guo, Y. Wan, H. Qin, Y. Jiang, T. Jaki, F.G. Hayden, P.W. Horby, B. Cao, C. Wang, Remdesivir in adults with severe COVID-19: a randomised, double-blind, placebo-controlled, multicentre trial, *Lancet* 395 (2020) 1569–1578.
- [5] R.C. Group, P. Horby, M. Mafham, L. Linsell, J.L. Bell, N. Staplin, J.R. Emberson, M. Wiselka, A. Ustianowski, E. Elmahi, B. Prudon, T. Whitehouse, T. Felton, J. Williams, J. Faccenda, J. Underwood, J.K. Baillie, L.C. Chappell, S.N. Faust, T. Jaki, K. Jeffery, W.S. Lim, A. Montgomery, K. Rowan, J. Tarning, J.A. Watson, N.J. White, E. Juszczak, R. Haynes, M.J. Landray, Effect of hydroxychloroquine in hospitalized patients with covid-19, *N. Engl. J. Med.* 383 (2020) 2030–2040.
- [6] P.W. Horby, M. Mafham, J.L. Bell, L. Linsell, N. Staplin, J. Emberson, A. Palfreeman, J. Raw, E. Elmahi, B. Prudon, C. Green, S. Carley, D. Chadwick, M. Davies, M.P. Wise, J.K. Baillie, L.C. Chappell, S.N. Faust, T. Jaki, K. Jeffery, W.S. Lim, A. Montgomery, K. Rowan, E. Juszczak, R. Haynes, M.J. Landray, Lopinavir–ritonavir in patients admitted to hospital with COVID-19 (RECOVERY): a randomised, controlled, open-label, platform trial, *Lancet* 396 (2020) 1345–1352.
- [7] Kai Kupferschmidt, Remdesivir and interferon fall flat in WHO's megastudy of COVID-19 treatments. <https://www.sciencemag.org/news/2020/10/remdesivir-and-interferon-fall-flat-who-s-megastudy-covid-19-treatments>. (Accessed 16 May 2021).
- [8] World Health Organization, WHO Coronavirus (COVID-19) Dashboard, 20, <https://covid19.who.int/>. (Accessed May 2021).
- [9] Reuters, At least 194 countries have started vaccinating against COVID-19. <https://graphics.reuters.com/world-coronavirus-tracker-and-maps/vaccination-rollout-and-access/>. (Accessed 16 May 2021).
- [10] S.M. Kissler, C. Tedijanto, E. Goldstein, Y.H. Grad, M. Lipsitch, Projecting the transmission dynamics of SARS-CoV-2 through the postpandemic period, *Science* 368 (2020) 860–868.
- [11] B. Hu, H. Guo, P. Zhou, Z.-L. Shi, Characteristics of SARS-CoV-2 and COVID-19, *Nat. Rev. Microbiol.* 19 (2021) 141–154.
- [12] P. V'kovski, A. Kratzel, S. Steiner, H. Stalder, V. Thiel, Coronavirus biology and replication: implications for SARS-CoV-2, *Nat. Rev. Microbiol.* 19 (2021) 155–170.
- [13] Marco Cascella, Michael Rajnik, Abdul Aleem, Scott C. Dulebohn, Raffaella Di Napoli, Features, Evaluation, and Treatment of Coronavirus (COVID-19) [Updated 2021 Apr 20]. In: StatPearls [Internet], StatPearls Publishing, Treasure Island (FL), 2021 Jan. Available from: <https://www.ncbi.nlm.nih.gov/books/NBK554776/>. (Accessed 16 May 2021).
- [14] M.A. Tortorici, D. Veisler, Chapter Four - structural insights into coronavirus entry, in: F.A. Rey (Ed.), *Advances in Virus Research*, Academic Press, 2019, pp. 93–116.
- [15] L. Mousavizadeh, S. Ghasemi, Genotype and phenotype of COVID-19: their roles in pathogenesis, *J. Microbiol. Immunol. Infect.* 54 (2021) 159–163.
- [16] V.M. Corman, D. Muth, D. Niemeyer, C. Drosten, Chapter eight - hosts and sources of endemic human coronaviruses, in: M. Kielian, T.C. Mettenleiter, M.J. Roossinck (Eds.), *Advances in Virus Research*, Academic Press, 2018, pp. 163–188.
- [17] D.X. Liu, J.Q. Liang, T.S. Fung, Human coronavirus-229e, -OC43, -NL63, and -HKU1 (Coronaviridae), *Encycl. Virol.* (2021) 428–440.
- [18] L. Shen, Y. Yang, F. Ye, G. Liu, M. Desforges, P.J. Talbot, W. Tan, Safe and sensitive antiviral screening platform based on recombinant human coronavirus OC43 expressing the luciferase reporter gene, *Antimicrob. Agents Chemother.* 60 (2016) 5492–5503.
- [19] E. Smertina, N. Urakova, T. Strive, M. Frese, Calicivirus RNA-dependent RNA polymerases: evolution, structure, protein dynamics, and function, *Front. Microbiol.* 10 (2019), 1280–1280.
- [20] J. Wu, W. Liu, P. Gong, A structural overview of RNA-dependent RNA polymerases from the flaviviridae family, *Int. J. Mol. Sci.* 16 (2015) 12943–12957.
- [21] A. Mishra, A.S. Rathore, RNA dependent RNA polymerase (RdRp) as a drug target for SARS-CoV2, *J. Biomol. Struct. Dyn.* (2021) 1–13.
- [22] F. Picarazzi, I. Vicenti, F. Saladini, M. Zazzi, M. Mori, Targeting the RdRp of emerging RNA viruses: the structure-based drug design challenge, *Molecules* 25 (2020) 5695.
- [23] T. Kumar D, N. Shaikh, U. Kumar S, G.P. Doss C, H. Zayed, Structure-based virtual screening to identify novel potential compound as an alternative to remdesivir to overcome the RdRp protein mutations in SARS-CoV-2, *Front Mol Biosci* 8 (2021), 645216–645216.
- [24] A. Gharbi-Ayachi, S. Santhanakrishnan, Y.H. Wong, K.W.K. Chan, S.T. Tan, R.W. Bates, S.G. Vasudevan, A. El Sahili, J. Lescar, Non-nucleoside inhibitors of zika virus RNA-dependent RNA polymerase, *J. Virol.* 94 (2020) e00794–00720.
- [25] J. Ahmad, S. Ikram, F. Ahmad, I.U. Rehman, M. Mushtaq, SARS-CoV-2 RNA Dependent RNA polymerase (RdRp)-A drug repurposing study, *Heliyon* 6 (2020), e04502.
- [26] S. Santander Ballestín, D. Gómez Martín, S. Lorente Pérez, M.J. Luesma Bartolomé, Hepatitis C: a pharmacological therapeutic update, *J. Clin. Med.* 10 (2021) 1568.
- [27] I. Gentile, E. Zappulo, A.R. Buonomo, A.E. Maraolo, G. Borgia, Beclabuvir for the treatment of hepatitis C, *Expert Opin. Invest. Drugs* 24 (2015) 1111–1121.
- [28] M. El Kassas, T. Elbaz, E. Hafez, M.N. Wafi, G. Esmat, Discovery and preclinical development of dasabuvir for the treatment of hepatitis C infection, *Expert Opin. Drug Discov.* 12 (2017) 635–642.
- [29] Y. Furuta, T. Komeno, T. Nakamura, Favipiravir (T-705), a broad spectrum inhibitor of viral RNA polymerase, *Proc. Jpn. Acad. Series B* 93 (2017) 449–463.
- [30] R. Barr, C.A. Green, C.J. Sande, S.B. Drysdale, Respiratory syncytial virus: diagnosis, prevention and management, *Therapeutic Adv. Infect. Dis.* 6 (2019), 2049936119865798.
- [31] S.O. Aftab, M.Z. Ghouri, M.U. Masood, Z. Haider, Z. Khan, A. Ahmad, N. Munawar, Analysis of SARS-CoV-2 RNA-dependent RNA polymerase as a potential therapeutic drug target using a computational approach, *J. Transl. Med.* 18 (2020) 275.
- [32] R. Kumar, S. Mishra, Shreya, S.K. Maurya, Recent advances in the discovery of potent RNA-dependent RNA-polymerase (RdRp) inhibitors targeting viruses, *RSC Med. Chem.* 12 (2021) 306–320.
- [33] L. Tian, T. Qiang, C. Liang, X. Ren, M. Jia, J. Zhang, J. Li, M. Wan, X. YuWen, H. Li, W. Cao, H. Liu, RNA-dependent RNA polymerase (RdRp) inhibitors: the current landscape and repurposing for the COVID-19 pandemic, *Eur. J. Med. Chem.* 213 (2021) 113201.
- [34] C.N.S. Allen, S.P. Arjona, M. Santerre, B.E. Sawaya, Potential use of RNA-dependent RNA polymerase (RdRp) inhibitors against SARS-CoV2 infection, *Life* 13 (2020) 608–614.
- [35] G.N. Zhang, Q. Li, J. Zhao, X. Zhang, Z. Xu, Y. Wang, Y. Fu, Q. Shan, Y. Zheng, J. Wang, M. Zhu, Z. Li, S. Cen, J. He, Y. Wang, Design and synthesis of 2-((1H-indol-3-yl)thio)-N-phenyl-acetamides as novel dual inhibitors of respiratory syncytial virus and influenza virus A, *Eur. J. Med. Chem.* 186 (2020) 111861.
- [36] X. Zhang, G.N. Zhang, Y. Wang, M. Zhu, J. Wang, Z. Li, D. Li, S. Cen, Y. Wang, Synthesis and biological evaluation of substituted indole and its analogs as influenza A virus inhibitors, *Chem. Biodivers.* 16 (2019), e1800577.
- [37] F. Ferron, L. Subissi, A.T. Silveira De Morais, N.T.T. Le, M. Sevajol, L. Gluais, E. Decroly, C. Vonnrhein, G. Bricogne, B. Canard, I. Imbert, Structural and molecular basis of mismatch correction and ribavirin excision from coronavirus RNA, *Proc. Natl. Acad. Sci. Unit. States Am.* 115 (2018) E162.
- [38] J. Zhao, S. Guo, D. Yi, Q. Li, L. Ma, Y. Zhang, J. Wang, X. Li, F. Guo, R. Lin, C. Liang, Z. Liu, S. Cen, A cell-based assay to discover inhibitors of SARS-CoV-2 RNA dependent RNA polymerase, *Antivir. Res.* 190 (2021), 105078.
- [39] D.X. Hu, P. Grice, S.V. Ley, Rotamers or diastereomers? An overlooked NMR solution, *J. Org. Chem.* 77 (2012) 5198–5202.
- [40] P. Oguadinma, F. Bilodeau, S.R. LaPlante, NMR strategies to support medicinal chemistry workflows for primary structure determination, *Bioorg. Med. Chem. Lett* 27 (2017) 242–247.
- [41] Q. Li, D. Yi, X. Lei, J. Zhao, Y. Zhang, X. Cui, X. Xiao, T. Jiao, X. Dong, X. Zhao, H. Zeng, C. Liang, L. Ren, F. Guo, X. Li, J. Wang, S. Cen, Corilagin inhibits SARS-CoV-2 replication by targeting viral RNA-dependent RNA polymerase, *Acta Pharm. Sin. B* (2021), <https://doi.org/10.1016/j.apsb.2021.02.011>. In press.